이학박사 학위논문

# Synthesis of Block Copolymer Micelles for Supracolloidal Chains and Surface-Functionalized Nanoparticles

초구조콜로이드 사슬 및 표면이 기능화된
나노입자 제조를 위한 블록공중합체
마이셀의 합성

2016년 8월

서울대학교 대학원

화학부 고분자화학

이 상 화

# Synthesis of Block Copolymer Micelles for Supracolloidal Chains and Surface-Functionalized Nanoparticles

지도 교수 손 병 혁

이 논문을 이학박사 학위논문으로 제출함

2016 년 6 월

서울대학교 대학원

화학부 고분자화학

이 상 화

이상화의 이학박사 학위논문을 인준함

2016 년 6 월

| | | |
|---|---|---|
| 위 원 장 | 정 택 동 | (인) |
| 부위원장 | 손 병 혁 | (인) |
| 위 원 | 박 승 범 | (인) |
| 위 원 | 김 경 택 | (인) |
| 위 원 | 송 오 성 | (인) |

## Abstract

# Synthesis of Block Copolymer Micelles for Supracolloidal Chains and Surface-Functionalized Nanoparticles

**Sanghwa Lee**

**Department of Chemistry**

**The Graduate School**

**Seoul National University**

Self-assembled nano-building blocks into controlled superstructures is of significant importance in technological applications as well as of great interest in basic science because cooperative electronic, photonic, and magnetic properties of individual nano-objects are determined by the collective interactions in their ensembles. In particular, uniform nanoparticles of metals, semiconductors, oxides,

and polymers have been assembled into supracolloidal assemblies upon the controlled attraction between nanoparticles. Especially, patchy nanoparticles have been employed as colloidal building blocks which can be effectively polymerized into linear supracolloidal chains.

Colloidal particles with well-ordered patches have been developed mainly for mimicking the valency in an atomic structure to demonstrate an artificial atom in the large scale. However, colloidal particles with multivalent patches have not been utilized for controlling branching or crosslinking. In addition, it would not be trivial to synthesize colloidal patchy particles smaller than 100 nm.

In this thesis, we focus on the controlled branching and eventual crosslinking in supracolloidal chains by introducing well-defined trifunctional patchy micelles. Three patches in the micelles worked as the distinct parts for crosslinking as well as branching, analogues to multifunctional groups in classical gelation of small molecular monomers. These branched and crosslinked supracolloidal chains were well compared with long linear chains only with bifunctional micelles. Furthermore, we carried real visual images on branching and crosslinking in chain-like structures which cannot be directly imaged in conventional gelation of small multifunctional monomers. We also demonstrate that diblock copolymer micelles can be used as surface-functionalized particles and they can be coated with Ag or $TiO_2$ nanoparticles without surface modification. We obtained dopamine-functionalized diblock copolymers which were synthesized by the

reversible addition fragmentation chain transfer polymerization and followed by the post-polymerization modification. By dissolving this amphiphilic diblock copolymer in water, spherical micelles with the dopamine-functionalized coronas were induced, which are essentially equivalent to polymeric particles with dopamine-functionalized surface.

Chapter 1 gives a brief overview of the self-associating characteristics of diblock copolymers, which assemble into micelles with soluble coronas and insoluble cores in a selective solvent for one of the blocks. The structure and dimension of block copolymer micelles can be precisely tuned by the molecular weight of polymers and the weight ratio of the blocks. These diblock copolymer micelles can be potentially employed as nano-sized polymeric colloids. The synthesis and post-polymerization modification of block copolymers for functionalization is also introduced.

In Chapter 2, we demonstrate that controlled branching and eventual crosslinking in supracolloidal chains by introducing well-defined trifunctional patchy micelles. Uniform micelles having three patches were induced from core-crosslinked micelles of diblock copolymers. Three patches in the micelles served as functional groups for crosslinking as well as branching in supracolloidal polymerization with bifunctional patchy micelles. Thus, by the addition of trifunctional micelles, supracolloidal chains showed branches originated only from the trifunctional units and were eventually crosslinked into the network

structure, in sharp contrast to long linear chains of bifunctional patchy micelles. Formation of crosslinked supracolloidal chains of patchy micelles was understood by the classical gelation theory. We also delivered visual images on branching and crosslinking in chain-like structures which cannot be directly imaged in conventional gelation of small multifunctional monomers.

In Chapter 3, we describe that diblock copolymer micelles can be used as surface-functionalized particles and they can be coated with Ag or $TiO_2$ nanoparticles without surface modification. We first obtained dopamine-functionalized diblock copolymers which were synthesized by the reversible addition fragmentation chain transfer polymerization and followed by the post-polymerization modification. By dissolving this amphiphilic diblock copolymer in water, spherical micelles with the dopamine-functionalized coronas were induced, which are essentially equivalent to polymeric particles with dopamine-functionalized surface. Thus, without additional surface functionalization, we were able to directly decorate these particles with Ag and $TiO_2$ nanoparticles due to the dopamine functionality on their surface.

**Keywords : Diblock Copolymer, Self-assembly, Supracolloidal Polymer, Branched Structure, Network Structure, Surface Functionalization, Nanoparticle, Dopamine**

**Student Number : 2012-30878**

## Contents

Abstract ..... 1

Contents ..... 6

List of Figures ..... 8

**Chapter I. Introduction** ..... 11

1.1 Motivation ..... 12

1.2 Block Copolymers ..... 17

1.3 Self-Assembly of Block Copolymers Micelles ..... 19

1.4 Synthesis of Block Copolymers ..... 23

1.5 Post-Polymerization for Modification of Block Copolymers ..... 24

1.6 References ..... 26

**Chapter II. Branched and Crosslinked Supracolloidal Chains with Diblock Copolymer Micelles having Well-defined Three Patches** ..... 40

2.1 Introduction ..... 41

2.2 Experimental Section ..... 45

2.3 Results and discussion ..... 50

2.4 Conclusion ..... 62

2.5 References..... 63

**Chapter III. Diblock Copolymer Micelles as Surface-Functionalized Particle and Direct Decoration of Nanoparticles** ..... 77

3.1 Introduction..... 78

3.2 Experimental..... 81

3.3 Results and discussion ..... 87

3.4 Conclusions..... 90

3.5 References..... 91

# List of Figures

**Chapter I**

Figure 1-1. Common morphologies of microphase-separated block copolymers: body centered cubic (bcc) packed spheres (BCC), hexagonally ordered cylinders (HEX), gyroid (Ia3d), hexagonally perforated layers (HPL), modulated lamellae (MLAM), lamellae (LAM), cylindrical micelles (CYL), and spherical micelles (MIC)

Figure 1-2. $\chi N$ versus $f_{PI}$ diagram for PI-*b*-PS diblock copolymers. Open and filled circles represent the order-order (OOT) and order-disorder (ODT) transitions, respectively. The dash-dot curve is the mean field prediction for the ODT. Solid curves have been drawn to delineate the different phases observed but might not correspond to precise phase boundaries. Five different ordered microstructures (shown schematically) have been observed for this chemical system.

Figure 1-3. Schematic representation of AB diblock copolymer micelles in a selective solvent of the A block. $R_c$ : core radius; L : shell(corona) thickness.

Figure 1-4. Mechanism of RAFT polymerization

**Chapter II**

Figure 2-1. TEM images: (a) PS(41k)-*b*-P4VP(24k) micelles having three patches; (b) PS(51k)-*b*-P4VP(18k) micelles having two patches. The scale bars are 200 nm. Each inset is an enlarged image (80 nm × 80 nm) of an individual micelle. $RuO_4$ and $I_2$ stained the PS patches (left inset) and the P4VP core (right inset), respectively.

Figure 2-2. Micelles with two and three patches depending on the total

molecular weight and the volume ratio of PS to P4VP.

Figure 2-3. TEM images: (a) linear chains of bifunctional micelle; (b) branched chains by adding 5.0 % trifunctional micelles. The PS block was stained with $RuO_4$. The scales bars are 300 nm. All insets are 2-fold enlarged images. Trifunctional micelles in the insets are indicated by arrows.

Figure 2-4. TEM images after 48 h supracolloidal polymerization: (a) a long linear chain of bifunctional micelles; (b) crosslinked chains by adding 5.0 % trifunctional micelles. The P4VP block was stained with $I_2$. The scales bars are 300 nm. The insets are 2-fold enlarged images stained with $RuO_4$. The arrows indicate trifunctional micelles.

Table 2-1. List of PS-b-P4VP with volume ratios of PS to P4VP and patch numbers. The number in the parentheses is a molecular weight in g/mol.

Figure 2-5. Spherical micelles of (a) PS(41k)-*b*-P4VP(24k) and (b) PS(51k)-*b*-P4VP(18k): (left column) diameter distributions by DLS; (center column) TEM images after $RuO_4$ staining; (right column) diameter histograms from TEM images. The scale bars in the TEM images are 200 nm. The insets are enlarged images (100 nm × 100 nm) of micelles stained with $RuO_4$ (left) and $I_2$ (right).

Figure 2-6. TEM images of small and large micelles having three patches: (a) PS(21k)-*b*-P4VP(13k); (b) PS(41k)-*b*-P4VP(24k). PS patches were stained with $RuO_4$. The scale bars are 100 nm.

Figure 2-7. TEM images of micelles having two and three patches. The size of each image is 450 nm × 450 nm. P4VP cores were stained with $I_2$.

Table 2-2. . Micelles of PS(51k)-b-P4VP(18k) (left) and PS(41k)-b-P4VP(24k) (right) in toluene mixed with polar solvents having various solubility parameters (δs). The size of each TEM image is 80 nm × 80 nm. Micelles were stained with $RuO_4$. Figure 2-8. SEM image of a linear supracolloidal chain of PS(51k)-*b*-P4VP(18k). The scale bar is 200 nm.

Figure 2-8. TEM images after 12 h supracolloidal polymerization of patchy micelles of PS(51k)-b-P4VP(18k) by adding different amounts of water: (a) 12.5 wt%; (b) 20.0 wt%; (c) 27.5 wt%. The P4VP block was stained with $I_2$. The scales bars are 300 nm.

Figure 2-9. TEM image after 12 h supracolloidal polymerization of patchy micelles of PS(51k)-b-P4VP(18k) by adding 12.5 wt% polar solvent instead of water: (a) methanol; (b) ethylene glycol. The P4VP block was stained with $I_2$. The scales bars are 300 nm.

Figure 2-10. TEM images of long linear supracolloidal chains of bifunctional micelles with various DPs. The number with each chain is the DP of the chain. The scale bar is 500 nm.

Figure 2-11. (a) Size distributions of supracolloidal chains of bifunctional micelles of PS(51k)-b-P4VP(18k) after various polymerization hours; (b) Linear dependence of the size on the polymerization time.

**Chapter III**

Figure 3-1. Synthesis of dopamine-functionalized PDA-b-PS from PPFPA-b-PS.

Figure 3-2. Size distribution of PDA-b-PS micelles by DLS measurements.

Figure 3-3. SEM and TEM (inset) images of PDA-b-PS micelles.

Figure 3-4. SEM image of PS particles decorated with Ag nanoparticles by

utilizing PDA-b-PS micelles as dopamine-functionalized PS particles. The inset is an enlarged image.

Figure 3-5. UV-Vis spectra of PS particles decorated with nanoparticles: (a) Ag; (b) $TiO_2$.

Figure 3-6. SEM image of PS particles with $TiO_2$ nanoparticles. The inset is a TEM image.

Figure 3-7. TEM images of PDA-b-PS micelles; (a) 4K-23K, (b) 9K-67K, (c) 4K-62K

# Chapter I.

# Introduction

## 1-1. Motivation

The rapidly developing field of nanotechnology requires novel materials with increasingly complex. Despite the complexity achieved in nature through self-assembly, the actual pool of nano-building blocks used is relatively small. Self-assembly defines the spontaneous organization of nano-building blocks into larger structures with well-defined symmetry, complex architecture. As a versatile tool for the energy-efficient bottom-up structuring of bulk materials, surface patterns or nano objects in solution[1-5], self-assembly fuels the innovative design of nanomaterials that are “smart”, self-healing, programmed for target-oriented motion, and serve as miniaturized components for nanoelectronics or nanooptics.[6-14] Complexity arises from the self-assembly of these nano-building blocks using a variety of molecular interactions, for example electrostatic, hydrogen bonding, metal–ligand and p-donor/acceptor, as well as many other covalent and non-covalent linkages.

Self-assemblies of block copolymers are potential candidates for use as nano-building blocks. Block copolymers, which have two or more chemically different homopolymers which are covalently bonded, spontaneously self-assemble into periodic nanostructures with a regular size and morphology.[15,16] Especially, in a selective solvent for one of the blocks, block copolymers self-organize into micelles with a soluble corona block and an insoluble core. The

dimensions of block copolymer micelles are precisely tunable on the nanometer scale by controlling the molecular weight. In addition, the shape of block copolymer micelles are controlled according to the volume ratio of the blocks.

Until now, two methodologies have been employed for effective fabrication of nanomaterials. The first one is called the top-down approach, which is starting from large substances, and scaling down them into smaller and smaller pieces on the basis of photolithographic operational principles.[17-20] The major draw-back of these methods is cost caused by complex processes and low through-put rates. The other way to create nanomaterials is the "bottom-up" approach via a "self-assembly", which is starting with individual atoms, or molecules and bringing them together to build nanoparticles, nanowires, thin films, and so on, in which every atom is in a precise and designed location. [21-23] Self-assembly technologies enabled to fabricate a variety of nanostructured materials in a controlled way not only on their size but also on their shapes like as spheres, rods, and tetrapods. [24-27] However, by pure self-assembly alone, it can't be easily achieved to locate nanomaterials effectively in a periodic or aperiodic arrangement on a solid substrate without aggregation, particularly over an extended area. Guided self-assembly of nanomaterials on topographically or chemically pre-patterned structures can be engaged to locate nanomaterials in a specific area on solid substrates. [28-33] However, these approaches require independent synthesis of nanomaterials and modification of surface characteristics of them for selective deposition. Furthermore, an arrangement of

nanomaterials without aggregation could require a careful control over experimental condition such as a concentration, an evaporation speed, and so on. Alternatively, self-assemblies of block copolymers have been successfully hired as engineered scaffolds for creating functional nanostructured materials in a controlled arrangement without independent fabrication and placement of nanomaterials on the substrate. [35-42] The nanofabrication technique based on block copolymers is a parallel process, resulting in an easy creation of functional nanostructures.

Self-assemblies of block copolymers are possible candidates for use as nanosized polymeric colloids. Block copolymers, which have two or more chemically different homopolymers which are covalently bonded, spontaneously self-assemble into periodic nanostructures with a regular size and morphology.[43-44] In a solvent that dissolves one of the blocks selectively, block copolymers self-associate into micelles with a soluble corona block and an insoluble core. The dimensions of block copolymer micelles are precisely tunable on the nanometer scale by controlling the molecular weight. In addition, the shape of block copolymer micelles are controlled to form spheres or cylinders according to the volume ratio of the blocks.[45]

Block copolymer micelles can be employed as colloidal containers which can include various functional nanomaterials, e.g. organic dyes and inorganic precursors which are insoluble in solvents, in their core blocks such that

they are beneficial as functional colloids when applied in further applications.[43,44,46,47] These functionalized block copolymer micelles can be transferred onto solid substrates by simple coating methods, such as Langmuir-Blodgett (LB), dipcoating, or spin-coating to form a variety of nanostructures.[43,48,49] Micellar nanostructures on solid substrates can be used as nanoscale lithographic mask in etching processes and as templates for the in-situ synthesis of nanoparticles of metal, semiconductors, or oxides into micellar cores with or without removal of the copolymer template.[50-52] Thus, block copolymer micelles can act as colloidal templates which can be used to arrange and organize ordered colloidal structures of other colloidal nanomaterials.

In this thesis, we focus on the development of organized structures of colloidal building blocks through the utilization of diblock copolymer micelles in a solution. We generated uniform patchy nanoparticles of diblock copolymer micelles having three patches. We found the range of volume ratios of corona to core in the micelles for dominant formation of three patches. Then, trifunctional nanoparticles of the micelles with three patches were polymerized into supracolloidal chains together with bifunctional micelles having two patches. By the addition of trifunctional micellar nanoparticles, supracolloidal chains showed controllable branches originated only from the trifunctional units and were eventually crosslinked into the network structure, in striking contrast to long linear supracolloidal chains in the case of polymerization only with bifunctional micelles. Formation of linear chains and networks of patchy micelles was

understood by the classical Carothers theory of polymerization and gelation. Since all supracolloidal chains here were clearly imaged by transmission electron microscopy, we were able to directly visualize branching and eventual crosslinking by the addition of trifunctional units, which can be only identified indirectly by mechanical or thermodynamic quantities in classical polymerization of small molecular monomers. We also demonstrate that by inducing spherical micelles of amphiphilic PDA-b-PS in water, we obtained PS particles having dopamine functionality on their surface without additional surface modification. Thus, we were able to directly decorate these PS particles with Ag and $TiO_2$ nanoparticles due to the dopamine functionality on their surface.

## 1-2. Block Copolymers

Block copolymers composed of two or more chemically different polymers, covalently linked, spontaneously self-assemble into larger structures, whether in bulk or in a solution. [53, 54] For diblock copolymers, which consist of two different polymers, the segregation of the block components due to thermodynamic incompatibility and the connectivity of the two chains produces various microdomains such as lamella, cylinder, sphere, and gyroid structures. [53] An overview over the most common structures that are formed by diblock copolymers is shown in Figure 1-1. [55] Such a variety of ordered nanostructures forms via the process of microphase separation. The size and morphology of microphase-separated domains can be determined by the molecular weight, the volume fraction of each block, and the Flory-Huggins interaction parameter, $\chi$. Here, $\chi$ is found to be inversely proportional to temperature and is usually parameterized as $\chi$ = A/T+B. Also, $\chi$ reflects the interaction energy between different segments. [53] At equilibrium the nanostructures of block copolymers are controlled by delicate balance between the entropic and the enthalpic energy contribution to minimize the overall free energy. The magnitude of the entropic energy contribution is largely determined by the degree of polymerization, $N$, while that of the enthalpic energy contribution is controlled predominantly by $\chi$(T). [53]

The product $\chi N$ that expresses the enthalpic-entropic balance is then used to parameterize block copolymer phase behavior, along with the composition of the copolymer. For a diblock copolymer, the volume fraction of one component, *f*, controls which ordered structures are accessed beneath the order-disorder transition (ODT). Depending on the degree of incompatibility $\chi N$, several regimes have been identified: the weak segregation limit (WSL) corresponds to $\chi N$ close to $(\chi N)_{ODT}$. In WSL regime, the composition profile is approximately sinusoidal, i.e. a broad interface with a composition profile. This regime encompasses the various ordered phases and the ordered phase close to the ODT. At much higher value of $\chi N$ ($\chi N >> 10$), the components are strongly segregated and each domain is almost pure, with a narrow interface between them. This is the strong segregation limit. For $\chi N << 1$ the system is disordered and microscopically homogeneous. [56]

A phase diagram constructed from experiments on a series of polystyrene-*block*-polyisoprene (PS-*b*-PI) diblock copolymers is presented in Figure 1-2. Five different ordered microstructures (shown schematically such as BCC sphere, hexagonal cylinder, gyroid, hexagonally perforated layer, lamellae) together with their inverse morphologies have been observed for this chemical system. [57]

## 1-3. Self-Assembly of Block Copolymer Micelles

As noted in the previous section, a diblock copolymer is composed of two chemically different polymers linked by a covalent bond. The microphase separation of diblock copolymers is managed by the enthalpy arising when mixing constituent blocks and the entropic penalty related to the chain length. These thermodynamic terms of enthalpy and entropy are proportional to the Flory-Huggings interaction parameter ($\chi$) and the degree of polymerization (N) respectively such that the phase behavior of block copolymers can be predicted by the product $\chi$N, which denotes the enthalpy-entropy balance. [58.59] With the segregation of dissimilar polymer blocks in a diblock copolymer, block copolymers are self-associated into structures with internal domains with nanoscale lengths. Self-assembled diblock copolymers form various nanostructures in a solution. [60-62]

Block copolymers in a diluted solution self-associate into micelles with coronas of the soluble block and cores of the insoluble block in a selective solvent that dissolves only one block above a concentration termed the criticial micelle concentration (cmc). [63] The size and structure of micelles are determined by the molecular weight of each block, the volume ratio between the blocks, the chemical affinity of each block to the solvent and the chemical miscibility between the blocks. [64]

A diblock copolymer is presented as A-B. In a selective solvent for B blocks, the micelle consists of an A-rich core and a B-rich corona. Depending on the domain sizes of the cores and coronas, two boundary models, hairy micelles and crew-cut micelles, have been introduced. In figure 1-3, a hairy micelle has a much larger corona than its core, whereas a crew-cut micelle has a larger core than its corona. [65, 66]

Regardless of whether the micellar structure is the hairy or crew-cut type, amphiphilic block copolymers form "amphiphilic micelles" composed of a core with only an A block and a corona with only a B block. The micellization of amphiphilic block copolymers is driven by the strong segregation of A and B blocks, which is characterized by a large interaction parameter $\chi N$ ($\gg$ 10) due to the energy penalty of the A-solvent interaction and the compatibility of the B solvent with high interfacial energy between the A-B blocks. [66]

We can introduce an aggregation number, Z, which is the number of block copolymer molecules in a micelle, to characterize the structure of diblock copolymer micelles. The aggregation number ($Z$) of amphiphilic micelles is proportional to the square of the degree of polymerization ($N^2$), corresponding to a strong segregation limit regime. [59, 66] Specifically, the aggregation number for amphiphilic molecules can be quantitatively expressed by the degree of polymerization of each block as in an earlier work. [66]

$$Z = Z_0 N_A^{\alpha} N_B^{\beta} \quad \text{(a)}$$

In this equation, $Z_0$ is related to the interaction parameter $\chi$ and the local packing parameter as expressed in the aforementioned study. [66]

$$Z_0 = 36\pi\Delta_0^3, \quad \Delta_0^3 = \frac{v_0^{2/3}}{b_0^3} \quad \text{(b)}$$

Here, $\Delta_0$ is a dimensionless intrinsic patching parameter of a specific block copolymer and solvent system. It is notable that equation a and b are universal in the system of strong segregating amphiphilic molecules including diblock, triblock and graft copolymers as well as low molecular surfactants. The aggregation number of various amphiphilic structures versus the degree of polymerization of the A block is fitted onto a single plot of the equation. [66] For many micellar systems, the exponents $\alpha$ and $\beta$ are close to 2.0 and 0.8, respectively. [66]

The aggregation number as calculated by equation a and b enable the calculation of the core radius ($R_c$) via the space filling condition for the core and the corona dimension ($D_h$) for the swollen block in good solvents, approximately, [66]

$$\frac{4\pi}{3} R_c^3 = ZN_A v_0 \quad \text{(c)}$$

$$D_h \approx Z^{0.2} N_B^{0.6} \quad \text{(d)}$$

where $\nu_0$ is the molar volume of core monomers. The relationship between the core and corona dimension of the micellar nanostructures and the degree of polymerization of the block copolymers implies the manipulation of the sizes of the micelles by the molecular weight of block copolymers. The value of $Z_0$ of a variety of block copolymers is tabulated such that the preparation of diblock copolymer micelles with desired dimensions of the core and the corona, as colloidal substances, is promising for further potential applications in colloidal systems.

## 1-4. Synthesis of Block Copolymers

Among the various block copolymerization processes that have been reported to achieve such structures, controlled radical polymerization appears to be a method of choice. This process has enlarged the possibility of molecular weight control to a wide variety of monomers which could not be polymerized by classical living anionic polymerization. [67] The most important processes are nitroxide-mediated polymerization (NMP), [68] transition metal-mediated controlled radical polymerization (ATRP), [69] and reversible addition fragmentation chain transfer polymerization (RAFT) [70]. NMP is based on the use of stable nitroxide radicals– mainly 2,2,6,6-tetramethylpiperidine-N-oxyl (TEMPO) and its derivatives–and, to date, is limited to only a few monomers (styrene derivatives, N,N-dimethylacrylamides, dienes, acrylonitriles). [67] In additional, the process only works satisfactorily at higher temperatures (120 to 150℃) and requires long polymerization times. ATRP has proven to polymerize a wider range of monomers, including styrene derivatives methacrylates, acrylonitrile, and methacrylamides.[71] a catalyst and, therefore, pollution of the final product, which is a drawback not only for a large scale process. Recently, Rizzardo and co-workers reported a new living radical polymerization technique that offers exceptional versatility. [72] This RAFT process seems so far the most promising of the living radical polymerization systems. (figure 1-4) [73] The easy

scale-up of the reaction and its compatibility with functional groups makes it a very suitable technique to obtain well-defined homo and block copolymers. Similarly to ATRP, residual chain transfer agent may remain in the polymer sample.

## 1-5. Post-polymerization for Modification of Block Copolymers

Recently, the demands of functional polymers that are specifically designed are rapidly growing in material science for specialized applications. [74] Despite the tremendous progress in the area of controlled polymerization techniques, direct polymerization often suffers from a limited functional group tolerance under the polymerization condition. However, it can be an effective approach that polymers are modified the reactive site with the desired function after polymerization. It is referred to as post-polymerization modification. [74] Since Sharpless and coworkers introduced the concept of ‘‘click’’ chemistry in 2001, [75] various reactive groups such as aldehyde, [76] azide, [77] and activated ester [78-80] have been applied for the functionalization of polymers by post-polymerization modification. More functional groups employed in poly-polymerization reactions are explained in the review article. [81, 82]

Particularly, vinyl monomers with an activated ester like pentafluorophenyl(meth)acrylate can be polymerized by RAFT polymerization with a

narrow distribution of molecular weights. [83, 84] The synthesized polymers with activated esters can be easily modified with good reactivity and are soluble in organic solvents. [79] For example, block copolymers containing activated esters were synthesized and modified for bio-compatible or stimulus-responsible micelles, [85, 86] and surface alteration of metal oxide nanorods or QDs. [87-89]

## 1-6. References


[1] G. M. Whitesides and B. Grzybowski, Science, **2002**, 295, 2418–2421.

[2] R. D. Kamien, Science, **2003**, 299, 1671–1673.

[3] S. Mann, Nat. Mater., **2009**, 8, 781–792.

[4] J. A. Pelesko, Self-Assembly: The science of things that put themselves together, Chapman & Hall/CRC, **2007**.

[5] F. H. Schacher, P. A. Rupar and I. Manners, Angew. Chem.,Int. Ed., **2012**, 51, 7898–7921.

[6] P. Fratzl and R. Weinkamer, Prog. Mater. Sci., **2007**, 52, 1263–1334.

[7] Z. Tang, Y. Wang, P. Podsiadlo and N. A. Kotov, Adv. Mater., **2006**, 18, 3203–3224.

[8] B. V. Slaughter, S. S. Khurshid, O. Z. Fisher, A. Khademhosseini and N. A. Peppas, Adv. Mater., **2009**, 21, 3307–3329.

[9] M. A. Cohen Stuart, W. T. S. Huck, J. Genzer, M. Müller, C. Ober, M. Stamm, G. B. Sukhorukov, I. Szleifer, V. V. Tsukruk, M. Urban, F. Winnik, S. Zauscher, I. Luzinov and S. Minko, Nat. Mater., **2010**, 9, 101–113.

[10] D. H. Gracias, J. Tien, T. L. Breen, C. Hsu and G. M. Whitesides, Science, **2000**, 289, 1170–1172.

[11] F. C. Simmel, A. O. Govorov and T. Liedl, Nature, **2012**, 483, 8–11.

[12] Y. Kang, J. J. Walish, T. Gorishnyy and E. L. Thomas, Nat. Mater., **2007**, 6, 957–960.

[13] E. R. Kay, D. A. Leigh and F. Zerbetto, Angew. Chem., Int. Ed., **2007**, 46, 72–191.

[14] S. Sengupta, M. E. Ibele and A. Sen, Angew. Chem., Int. Ed., **2012**, 51, 8434–8345.

[15] R. Glass, M. Möller, J. P. Spatz, Nanotechnology **2003**, 14, 1153.

[16] S. Föster, T. Plantenberg, Angew. Chem. Int. Ed. **2002**, 41, 689.

[17] Semiconductor lithography: principles and materials; Moreau, W. M; New York:

Plenum; **1988**.

[18] Ross, C. A.; Smith, H. I.; Savas, T.; Schattenburg, M.; Farhoud, M.; Walsh, M.; Abraham, M. C.; Ram, R. J. J. Vac. Sci. Technol. B. **1999**, 17, 3168.

[19] Choi, J. O.; Jeong, H. S.; Pflug, D. G.; Akinwande, A. I., Smith, H. I. Appl. Phys. Lett. **1999**, 74, 3050.

[20] Smith, H. I.; Schattenberg, M. L.; Hector, S, D.; Ferrera, J.; Moon, E. E.; Yang, I.Y.; Burkhardt, M. Microeelctron. Engng. **1996**, 32, 143.

[21] Nanoparticles and Nanostructured Films; Fendler, J. H., Ed.; Wiley-VCH: Weinheim, **1998**.

[22] Clusters and Colloids; Schmid, B., Ed.; VCH Press: New York, **1994**.

[23] Nanoscale Materials in Chemistry; Klabunde, K. J., Ed.; Wiley-Interscience: New York, **2001**.

[24] Weller, H. Angew. Chem. Int. Ed. **1993**, 32, 41.

[25] Hyeon, T. Chem. Commun. **2003**, 927.

[26] Puntes, V. F.; Krishnan, K. M.; Alivisatos, A. P. Science **2001**, 291, 2115.

[27] Murray, C. B.; Kagan, C. R.; Bawendi, M. G. Annu. Rev. Mater. Sci. **2000**, 30, 545.

[28] Qin, D.; Xia, Y.; Xu, B.; Yang, H.; Zhu, C.; Whitesides, G. M. Adv. Mater. **1999**,

11 1433.

[29] Chen, C.-C.; Lin, J.-J. Adv. Mater. **2001**, 13 136.

[30] He, H. X.; Zhang, H.; Li, Q. G.; Zhu, T.; Li, S. F. Y.; Liu, Z. F. Langmuir **2000**, 16, 3846.

[31] Lu, C.; Wu, N. ; Wei, F. ; Zhao, X. ; Jiao, X. ; Xu, J. ; Luo, C. ; Cao, W. Adv. Funct. Mater. **2003**, 13 548.

[32] Zhou, D.; Bruckbauer, A.; Abell, C.; Klenerman, D.; Kang, D.-J. Adv. Mater. **2005**, 17, 1243.

[33] Santhanam, V.; Andres, R. P. Nano Lett. **2003**, 4, 41.

[35] Bockstaller, M. R.; Mickiewicz, R. A.; Thomas, E. L. Adv. Mater. **2005**, 17, 1331.

[36] Haryono, A.; Binder, W. H. Small **2006**, 2, 600.

[37] Föster, S. Top. Curr. Chem. **2003**, 226, 1.

[38] Hamley, I. W. Nanotechnology **2003**, 14, R39.

[39] Park, C.; Yoon, J.; Thomas, E. L. Polymer **2003**, 44, 6725.

[40] Glass, R.; Möller, M.; Spatz, J. P. Nanotechnology **2003**, 14, 1153.

[41] Fasolka, M. J; Mayes, A. M. Annu. Rev. Mater. Res. **2001**, 31, 323.

[42] Föster, S.; Antonietti, M. Adv. Mater. **1998**, 10, 195.

[43] R. Glass, M. Möller, J. P. Spatz, Nanotechnology **2003**, 14, 1153.

[44] S. Föster, T. Plantenberg, Angew. Chem. Int. Ed. **2002**, 41, 689.

[45] A. Blanazs, S. P. Arms, A. J. Ryan, Macromol. Rapid Commun. **2009**, 30, 267.

[46] S. I. Yoo, S. H. Bae, K. S. Kim, B. H. Sohn, Soft Matter **2009**, 5, 2990.

[47] C. Li, J. Hu, S. Liu, Soft Matter **2012**, 8, 7096.

[48] S. Jain, F. S. Bates, Macromolecules **2004**, 37, 1511.

[49] A. Böker, A. H. E. Müller, G. Krausch, Macromolecules **2001**, 34, 7477.

[50] X. Li, K. H. A. Lau, D. H. Kim, W. Knoll, Langmuir **2005**, 21, 5212.

[51] W. J. Cho, Y. Kim, J. K. Kim, ACS Nano **2012**, 6, 249.

[52] S. H. Yun, S. I. Yoo, J. C. Jung, W. C. Zin, B. H. Sohn, Chem. Mater. **2006**, 18,

5646.

[53] Hamley, I. W. The Physics of Block Copolymers; Oxford University Press: New York, **1998**.

[54] Solvents and Self-Organization of Polymers; Webber, S. E.; Munk, P.; Tuzar, Z., Ed.; Kluwer Academic Publishers, Dordrecht, **1996**.

[55] Föster, S.; Antonietti, M. Adv. Mater. **1998**, 10, 195.

[56] Chen, C.-C.; Lin, J.-J. Adv. Mater. **2001**, 13 136.

[57] Khandpur, A. K.; Föster, S.; Bates, F. S.; Hamley, I. W.; Ryan, A. J.; Bras, W.; Almdal, K.; Mortensen, K. Macromolecules **1995**, 28, 8796.

[58] S. Föster, T. Plantenberg, Angew. Chem. Int. Ed. **2002**, 41, 689.

[59] F. S. Bates, G. H. Fredrickson, Annu. Rev. Phys. Chem. **1990**, 41, 525

[60] S. B. Darling, Prog. Polym. Sci. **2007**, 32, 1152.

[61] Y. Mai, A. Eisenberg, Chem. Soc. Rev. **2012**, 41, 5969.

[62] S. Förster, M. Konrad, J. Mater. Chem. **2003**, 13, 2671.

[63] G. Riess, Prog. Polym. Sci. **2003**, 28, 1107.

[64] E. B. Zhulina, M. Adam, I, LaRue, S. S. Sheiko, M. Rubinstein, Macromolecules **2005**, 38, 5330.

[65] M. Antonietti, S. Heinz, M. Schmidt, C. Rosenauer, Macromolecules **1994**, 27,

3276.

[66] S. Förster, M. Zisenis, E. Wenz, M. Antonietti, J. Chem. Phys. **1996**, 104, 9956.

[67] Rizzardo, E.; Chiefari, J.; R. Mayadunne , T. A. ‘‘Controlled Living Radical Polymerization–Progress in ATRP, NMPand RAFT’’, Matyjaszewski, K.; Ed., ACS Symposium Series 768, American Chemical Society, Washington, DC 2000, p. 278.

[68] Qiu, J.; Charleux, B.; Matyjaszewski, K. Prog. Polym. Sci. **2001**, 26, 2083.

[69] Schoen, F.; Hartenstein, M.; Mü ller, A. H. E. Macromolecules **2001**, 34, 5394.

[70] Barner-Kowollik, C.; Davis, T. P.; Heuts, J. P. A.; Stenzel, M. H.; Vana, P.; Whittaker, M. J. Polym. Sci., Part A: Polym. Chem. **2003**, 41, 365.

[71] Matyjaszewski, K.; Xia, J. H. Chem. Rev. **2001**, 101, 2921.

[72] Chiefri, J.; Chong, Y. K.; Ercole, F.; Krstina, J.; Jeffery, J.; Le, T. P. T.; Mayadunne, R. T. A.; Meijs, G. F.; Moad, C. L.; Moad, G.; Rizzardo, E.; Thang, S. H. Macromolecules **1998**, 31, 5559.

[73] Chong, Y. K.; Le, T. P. T.; Moad, G.; Rizzardo, E.; Thang, S. H. Macromolecules **1999**, 32, 2071.

[74] A. Das, P. Theato, Chem. Rev., **2016**, 116, 1434.

[75] H. C. Kolb, M. G. Finn, K. B. Sharpless, Angew. Chem. Int. Ed., **2001**, 40, 2004.

[76] R. C. Li, R. M. Broyer, H. D. Maynard, J. Polym. Sci. Part A: Polym. Chem., **2006**, 44, 5004.

[77] B. S. Sumerlin, N. V. Tsarevsky, G. Louche, R. Y. Lee, K. Matyjaszewski, Macromolecules, **2005**, 38, 7540.

[78] A. Godwin, M. Hartenstein, A. H. E. Müller, S. Brocchini, Angew. Chem. Int. Ed., **2001**, 40, 594.

[79] M. Eberhardt, R. Mruk, R. Zentel, P. Theato, Eur. Polym. J., **2005**, 41, 1569.

[80] P. Theato, J. Polym. Sci. Part A: Polym. Chem., **2008**, 46, 6677.

[81] R. K. Iha, K. L. Wooley, A. M. Nyström, D. J. Burke, M. J. Kade, C. J. Hawker, Chem. Rev., **2009**, 109, 5620.

[82] K. A. Günay1, P. Theato, H.-A. Klok, J. Polym. Sci. A : Polym. Chem., **2013**, 52, 1.

[83] M. N. Tahir, F. Natalio, H. A. Therese, A. Yella, N. Metz, M. R. Shah, E. Mugnaioli, R. Berger, P. Theato, H. C. Schröder, W. E. G. Müller, W. Tremel, Adv. Funct. Mater., **2009**, 19, 285.

[84] M. I. Shukoor, F. Natalio, M. N. Tahir, M. Wiens, M. Tarantola, H. A. Therese, M. Barz, S. Weber, M. Terekhov, H. C. Schröder, W. E. G. Müller, A. Janshoff, P. Theato, R. Zentel, L. M. Schreiber, W. Tremel, Adv. Funct. Mater., **2009**, 19, 3717.

[85] M. Barz, M. Tarantola, K. Fischer, M. Schmidt, R. Luxenhofer, A. Janshoff, P. Theato, R. Zentel, Biomacromolecules, **2008**, 9, 3114.

[86] F. Jochum, P. Theato, Chem. Comm., **2010**, 46, 6717.

[87] M. Zorn, M. N. Tahir, B. Bergmann, W. Tremel, C. Grigoriadis, G. Floudas, R. Zentel, Macromol. Rapid Commun., **2010**, 31, 1101.

[88] J. Kwak, W. K. Bae, M. Zorn, H. Woo, H. Yoon, J. Lim, S. W. Kang, S. Weber, H.-J. Butt, R. Zentel, S. Lee, K. Char, C. Lee, Adv. Mater., **2009**, 21 5022.

[89] L. zur Borg, D. Lee, J. Lim, W. K. Bae, M. Park, S. Lee, C. Lee, K. Char, R. Zentel, J Mater. Chem. C, **2013**, 1, 1722.

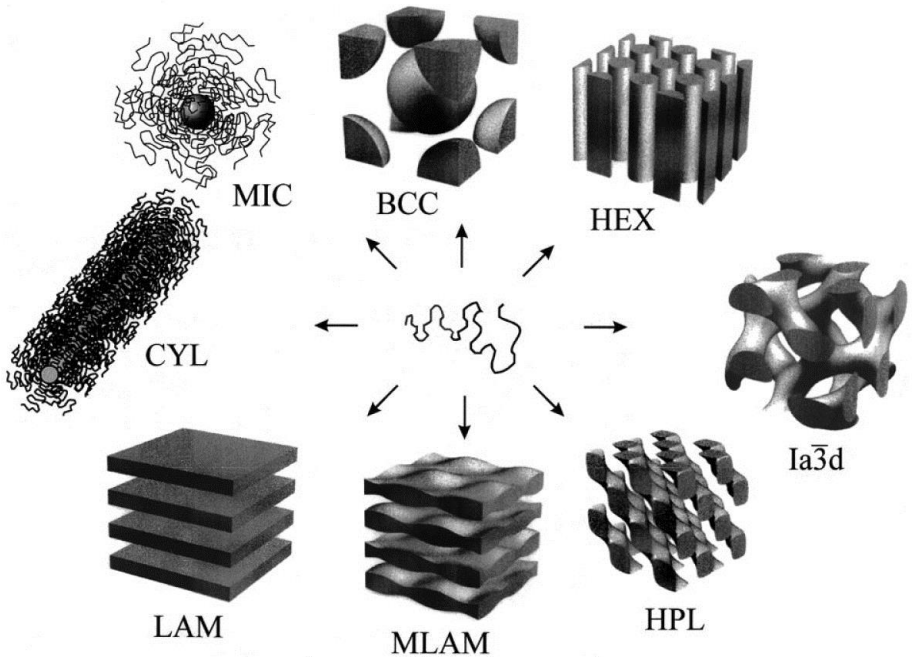


**Figure 1-1.** Common morphologies of microphase-separated block copolymers: body centered cubic (bcc) packed spheres (BCC), hexagonally ordered cylinders (HEX), gyroid (Ia3d), hexagonally perforated layers (HPL), modulated lamellae (MLAM), lamellae (LAM), cylindrical micelles (CYL), and spherical micelles (MIC). (Förster *et al.*, *Adv. Mater.*, **1998**, *10*, 195.)

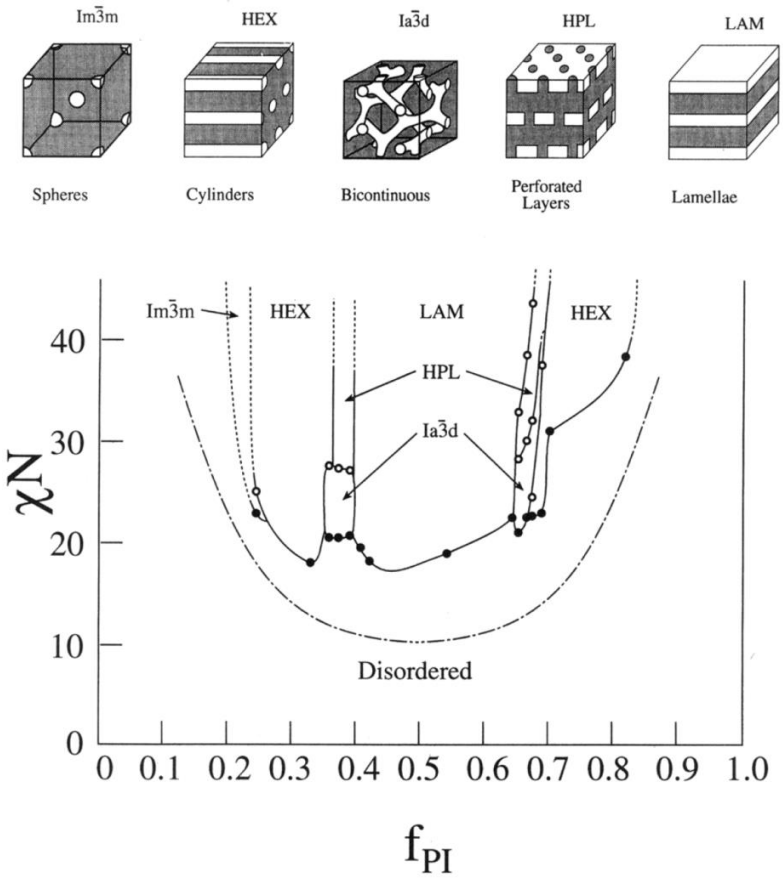


**Figure 1-2.** $\chi N$ versus $f_{PI}$ diagram for PI-*b*-PS diblock copolymers. Open and filled circles represent the order-order (OOT) and order-disorder (ODT) transitions, respectively. The dash-dot curve is the mean field prediction for the ODT. Solid curves have been drawn to delineate the different phases observed but might not correspond to precise phase boundaries. Five different ordered microstructures (shown schematically) have been observed for this chemical system. (Khandpur *et al. Macromolecules*, **1995**, *28*, 8796.)

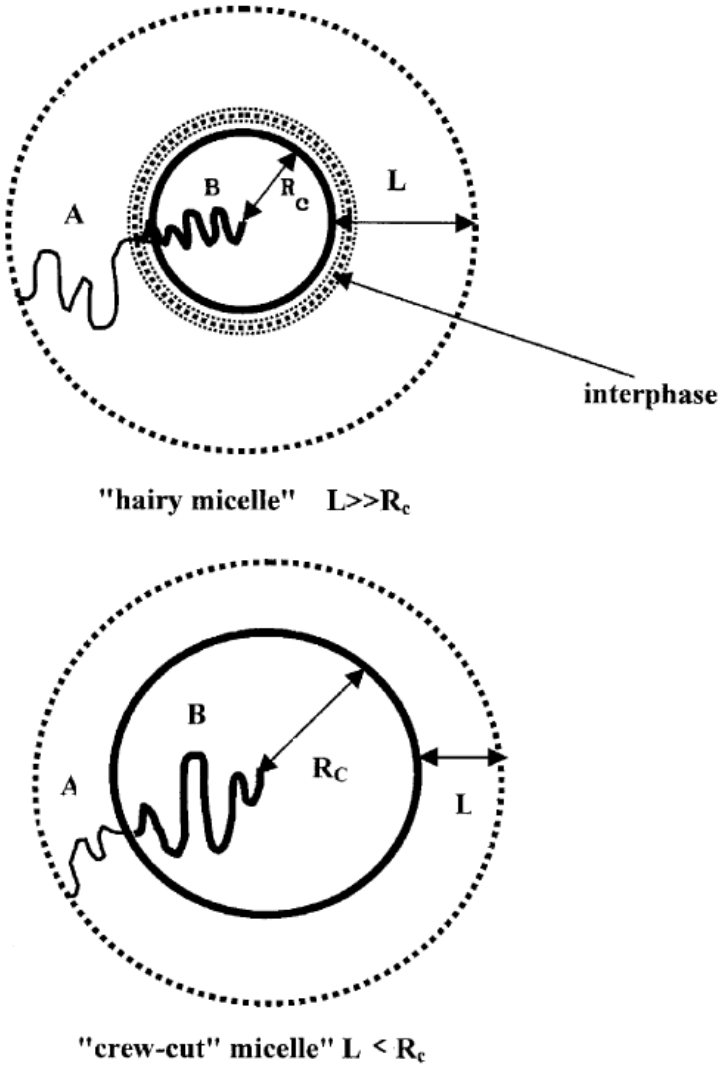


**Figure 1-3.** Schematic representation of AB diblock copolymer micelles in a selective solvent of the A block. Rc : core radius; L : shell(corona) thickness. (Riess *et al. Prog. Polym. Sci.*, **2003**, *28*, 1107.)

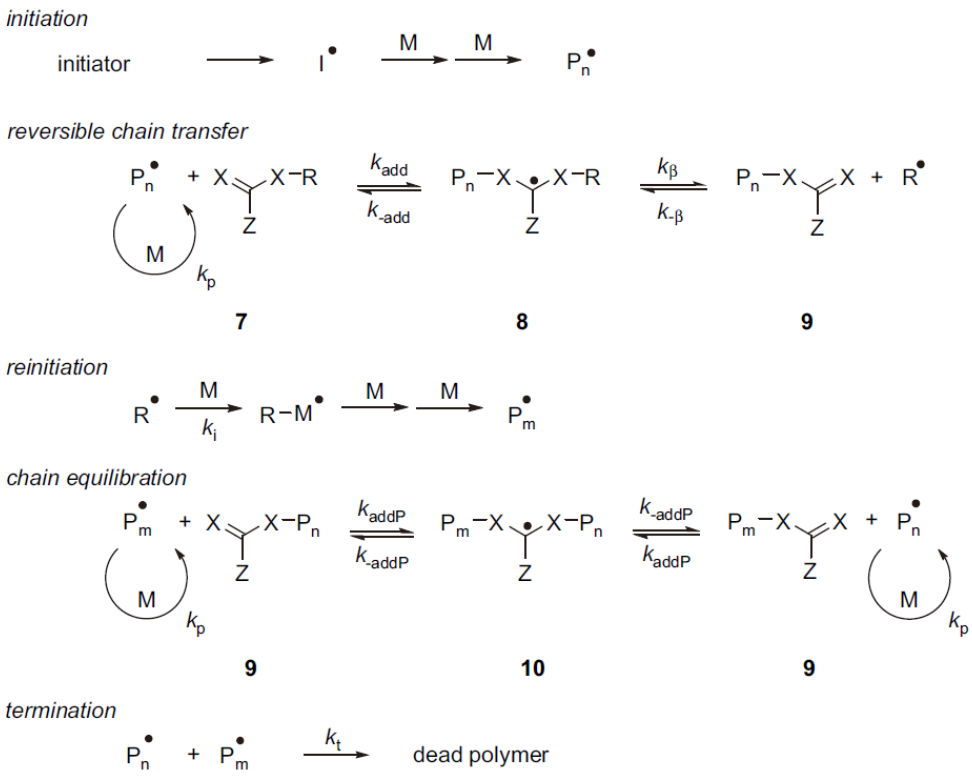


**Figure** 1-4. Mechanism of RAFT polymerization (G. Moad *et al. Polymer*, **2008**, 49, 1079.)

# Chapter II.

# Branched and Crosslinked Supracolloidal Chains with Diblock Copolymer Micelles having Well-defined Three Patches

## 2-1. Introduction

Assembling nanoscale building blocks into controlled superstructures is of considerable importance in technological applications as well as of great interest in basic science because cooperative electronic, photonic, and magnetic properties of individual nano-objects are determined by the collective interactions in their ensembles.[1-3] In particular, uniform nanoparticles of metals,[4,5] semiconductors,[6] oxides,[7.8] and polymers[9-11] have been assembled into supracolloidal assemblies upon the controlled attraction between nanoparticles. For example, linear chain-like assemblies of spherical nanoparticles were formed by electrostatic dipoles of quantum dots [12] or by spin dipoles of magnetic nanoparticles.[6,13] Modification of the surface characteristics of nanoparticles with functional groups[14-17] also enabled the formation of linear chain-like superstructures. Especially, patchy nanoparticles have been employed as colloidal building blocks which can be effectively polymerized into linear supracolloidal chains.[18-21] For instance, by the strategy of inducing directional attraction between the patches of neighboring nanoparticles with lateral repulsion to avoid non-directional aggregations, one-dimensional supracolloidal assemblies were demonstrated with nanorods having non-polar patches at two terminal facets[22] and with patchy micelles of triblock terpolymers consisting of the compartmentalized corona with polar patches and non-polar patches.[10] We

recently reported that anisotropic patchy micelles were induced from core-crosslinked micelles of diblock copolymers and polymerized into a supracolloidal chain by applying the same principle of directional attraction with orthogonal repulsion.[23,24]

In classical polymerization of monomers of small molecules, branched and crosslinked polymers beyond linear structures can be synthesized, particularly by introducing multifunctional monomers in step-growth polymerization.[25] In supracolloidal assemblies of nanoparticles, network structures as well as branched chains have been reported.[9, 26-28] For example, in ligand-induced assemblies of gold nanoparticles in two dissimilar sizes, the network structure was induced by connection of more than two nanoparticles onto one large nanoparticle which served as a crosslinking point.[26] Gold nanorods having two polymer patches at each end also assembled into chains having branches.[27] In patchy micelles of triblock terpolymers, relatively large patches in the compartmentalized corona attracted more than two micelles, resulting in supracolloidal networks.[9,28] In most cases, however, branching and crosslinking were formed without intentional controls, mainly because of ill-defined bonding sites in the multifunctional unit, for instance, the number of patches on patchy nanoparticles. If the number of patches and the patch size can be precisely controlled, nanoparticles having three or more patches can be co-assembled for the creation of branched or crosslinked supracolloidal chains in a controllable manner. Colloidal particles with well-ordered patches have been

developed mainly for mimicking the valency in an atomic structure to demonstrate an artificial atom in the large scale. [29-31] However, colloidal particles with multivalent patches have not been utilized for controlling branching or crosslinking. In addition, it would not be trivial to synthesize colloidal patchy particles smaller than 100 nm. By using triblock terpolymers [9, 28] or diblock copolymers,[32] multicompartment micelles with distinct patch numbers in regular sizes were generated, although their branching or crosslinking controllability in supracolloidal polymerization has not been demonstrated yet.

In this work, we first generated uniform patchy nanoparticles of diblock copolymer micelles having three patches. We found the range of volume ratios of corona to core in the micelles for dominant formation of three patches. Then, trifunctional nanoparticles of the micelles with three patches were polymerized into supracolloidal chains together with bifunctional micelles having two patches. By the addition of trifunctional micellar nanoparticles, supracolloidal chains showed controllable branches originated only from the trifunctional units and were eventually crosslinked into the network structure, in striking contrast to long linear supracolloidal chains in the case of polymerization only with bifunctional micelles. Formation of linear chains and networks of patchy micelles was understood by the classical Carothers theory of polymerization and gelation. Since all supracolloidal chains here were clearly imaged by transmission electron microscopy, we were able to directly visualize branching and eventual crosslinking by the addition of trifunctional units, which can be only identified

indirectly by mechanical or thermodynamic quantities in classical polymerization of small molecular monomers.

## 2-2. Experimental Section

*Materials*

Commercially available chemicals were used as received unless otherwise stated. $CaH_2$ (90~95%), benzyl dithiobenzoate (BDTB) (96%), n-hexane (96%), and N,N-dimethylformamide (DMF) (99.8%) were purchased from Aldrich. 2.2'-azoisobutyronitrile (AIBN) (95%) was acquired from Merck. AIBN was recrystallized with diethylether. Styrene (> 99%) and 4-vinylpyridine (4VP) (> 95%) were obtained from Aldrich. These monomers were passed through basic alumina columns to remove inhibitors and acidic impurities. Then, $CaH_2$ was added to the monomers, which were stirred overnight to eliminate traces of water. Monomers were further vacuum-distillated before polymerization. Polystyrene-b-poly(4-vinyl pyridine) (PS-b-P4VP) in Table 2-1 were synthesized by reversible addition-fragmentation chain transfer (RAFT) polymerization as described in the literature (*J. Polym. Sci., Part A: Polym. Chem.* **2012**, 50, 1636), except PS(51k)-b-P4VP(18k), PS(41k)-b-P4VP(24k), PS(25k)-b-P4VP(7k), PS(27k)-b-P4VP(7k), PS(48k)-b-P4VP(21k), and PS(33k)-b-P4VP(8k) which were purchased from Polymer Source and used without further purification. The number in the parenthesis is a number-average molecular weight in g/mol.

*Synthesis of PS-b-P4VP diblock copolymers*

We first synthesized the P4VP block by RAFT polymerization and then it was used as a macro chain transfer agent (CTA) to synthesize the additional PS block. A representative polymerization procedure is described below in the case of PS(21k)-b-P4VP(13k). A mixture of 4VP (10.0 g), BDTB (95 mg), AIBN (13 mg), and DMF (5.0 g) were added into a 50 mL Schlenk tube. This solution was degassed by three freeze-evacuate-thaw cycles and the tube was filled with nitrogen gas. The reaction tube was subsequently immersed in an oil bath at 65℃ for 8 h and then placed in an ice bath to stop the polymerization. The resulting mixture was diluted with THF (20 g). Then, this solution was slowly poured into an excess of n-hexane (500 g) to precipitate the polymer which was collected by filtration and then dried in a vacuum oven at room temperature for 48 h. We obtained P4VP (4.0 g) which was used as a macro CTA for the synthesis of the second PS block. We basically repeated the above procedure of RAFT polymerization for PS(21k)-b-P4VP(13k). We prepared a mixture solution of styrene (5.0 g), macro CTA of P4VP (0.46 g), AIBN (0.2 mg), and DMF (5.0 g). The polymerization was proceeded at 85℃ for 12 h. The polymerized mixture was diluted with DMF (5.0 g), instead of THF, before precipitation in n-hexane. After precipitation, filtration, and drying, we obtained PS(21k)-b-P4VP(13k) (1.5 g) in light pink.

*Formation of PS-b-P4VP micelles*

We first dissolved PS-b-P4VP copolymers (10.0 mg) in chloroform (1.0 g), a good solvent for both PS and P4VP blocks, to yield a 1.0 wt% solution. Then, we slowly added toluene (1.0 g), a selective solvent for the PS block, to the solution by a syringe pump at a rate of 30 ml/h. After mixing, chloroform was completely evaporated at 45℃ to obtain a 1.0 wt% toluene solution of PS-b-P4VP micelles. the same procedure was applied to all PS-b-P4VP in Table S1. To crosslink the P4VP core, 1,4-dibromobutane (DBB) (3.9 mg) was added to a toluene solution (1.0 g) containing the copolymer (0.01 g), yielding a molar ratio of DBB to 4VP equal to 0.5, which can fully quarternize the 4VP units in the copolymer, followed by stirring at 45℃ for 48 h. The amounts described in the parentheses are representative values for PS(21k)-b-P4VP(13k).

*Preparation of patchy micelles*

To produce colloidal monomers of patchy micelles, we changed the polarity of the solvent by adding DMF (9.9 g) to a 1.0 wt% toluene solution (0.1 g) of crosslinked PS-b-P4VP micelles by a syringe pump at a rate of 50 ml/h, resulting in a 0.01 wt% solution of patchy micelles of PS-b-P4VP. The same procedure was used for all PS-b-P4VP in Table 2-1

*Supracolloidal polymerization of patchy micelles*

We further increased the polarity of the solvent to synthesize supracolloidal chains of patchy micelles by dropping a mixture of DI water and anhydrous DMF (2.5 : 7.5 w/w) to yield 12.5 wt% water in the final solution. The solution was kept without stirring at 30℃ up to 48 h. For branched and crosslinked supracolloidal chains, we added 5% trifunctional micelles of PS(41k)-b-P4VP(24k) to a solution of patchy micelles of PS(51k)-b-P4VP(18k) and then followed the same procedure described above.

*Characterizations*

NMR spectra were obtained on a Varian NMR System (500 MHz). Gel permeation chromatography (GPC) was carried out on a Waters system (1515 pump, 2414 refractive index detector) with a Shodex GPC LF-804 column. Transmission electron microscopy (TEM) was performed on a Hitachi 7600 operating at 100 kV. A TEM sample was prepared by dropping a solution of micelles or supracolloidal chains on a carbon-coated TEM grid with removal of excess solvent by a filter paper. After drying in air, the TEM sample was exposed to $I_2$ and $RuO_4$ which stained P4VP and PS, respectively. Field-emission scanning electron microscopy (SEM) was performed on a Carl Zeiss SIGMA operating at

15 kV. Dynamic light scattering (DLS) analysis was carried out with an ALV/CGS-3 compact goniometer system.

## 2-3. Results and Discussion

For construction of supracolloidal chains with nano-building blocks such as metal nanoparticles, quantum dots, and copolymer micelles, a regular size of the building block with a narrow size distribution is compulsory. [1-3] Irregularity in the size of building blocks is normally amplified during their assembling procedure so that a linear chain-like structure is hardly achieved with non-uniform building blocks. Thus, we started with uniform spherical micelles consisting of the PS corona and the P4VP core using PS-b-P4VP diblock copolymers. PS(41k)-b-P4VP(24k) was initially selected, where the number in the parenthesis is a number-average molecular weight in g/mol. The volume ratio of PS to P4VP ($V_{PS}/V_{P4VP}$) of this copolymer is calculated as 1.87 by using the densities of 1.05 and 1.15 g/cm$^3$ for PS and P4VP, respectively. This ratio mainly governs a number of patches per micelle and will be discussed later.

To produce uniform micelles, we induced micelles with a step-by-step process. [23,24] We first dissolved PS(41k)-b-P4VP(24k) homogenously in chloroform and slowly added toluene, a PS-selective solvent, to a chloroform solution of the copolymer. After evaporation of chloroform, we obtained a toluene solution of PS(41k)-b-P4VP(24k) micelles. The diameter of the micelles was evaluated not only by dynamic light scattering (DLS) in a solution state but also by transmission electron microscopy (TEM) in a dried state (Figure 2-5) that directly showed spherical micelles with an average diameter of 60.5 nm with a narrow distribution

(±4.5 nm).

For creation of patchy micelles, we followed the procedure developed in our previous reports.[23,24] The strategy was converting a spherical micelle into a rearranged nanostructure having separated coronas initiated by the exposure of the crosslinked core to a favorable solvent which divides the corona into segregated patches, i.e., a popup structure of the core over the divided corona. Thus, crosslinking of the micellar core was the first step so that the P4VP cores of PS(41k)-b-P4VP(24k) micelles were crosslinked with 1,4-dibromobutane (DBB). Then, DMF, a good solvent for P4VP but a poor solvent for PS, was added to a toluene solution of the crosslinked micelles. The central P4VP core became directly exposed to DMF by rearranging the PS corona into segregated patches, resulting in micelles having separated PS patches. By this procedure, we mainly observed PS-b-P4VP micelle having two PS patches in our previous reports.23,24 In striking contrast, we obtained the micelles having three patches in the case of PS(41k)-b-P4VP(24k) as shown in Figure 2-1(a).

PS patches were selectively stained with RuO4 and appeared as dark spheres in the TEM image of Figure 2-1(a). Three dark spherical patches are connected each other with an angel of about $120^{o}$, which are clearly visible in the enlarged image of a single micelle (left inset). The bright P4VP core is discernible between the patches, indicating the direct exposure of the core to the solvent. We further visualized the P4VP core with selective $I_2$ staining (right inset), showing that the

core is still close to spherical shape and a large portion of the core is covered by three patches. The micellar radius (from the center to the one end of three patches) is estimated as ~31.6 nm with the patch radius of ~14.1 nm. Since we started with uniform spherical micelles, the micelles with three patches shown in Figure 2-1(a) are regular with respect to the micellar radius. We emphasize that patchy nanoparticles smaller than 100 nm with well-defined three patches were rarely reported and crucial to produce branched and crosslinked supracolloidal chains in a controlled manner, which will be demonstrated below. It is noted that micelles having two patches were inevitably formed and can be found in Figure 2-1(a), of which the amount was 1.9 % (19 micelles when 1000 micelles counted). We also note that three patches in some micelles are unequal in their sizes.

As mentioned earlier, $V_{PS}/V_{P4VP}$ of PS(41k)-b-P4VP(24k) is 1.87, smaller than 3.10 of PS(51k)-b-P4VP(18k), of which micelles have two patches, used in Figure 2-1(b) as well as in our previous reports.[23,24] To make direct contact between the core and the core-favorable solvent, a mode of the exposure of the core by dividing the corona can depend on the amount of the corona which initially screens the core from the solvent. In the case of micelles with a small amount of the corona compared to the core, i.e., small $V_{PS}/V_{P4VP}$, the corona can be easily divided into several parts, which become patches, by driving force of the interaction between the core and the core-favorable solvent. With a large amount of the corona compared to the core, i.e., a large value of $V_{PS}/V_{P4VP}$, the corona segregation cannot be easily initiated so that the corona may be divided

into a less number of patches. We assume that three patches can be dominantly formed with $V_{PS}/V_{P4VP}$ of 1.87. In order to exam the validity of this scenario for the patch formation, we employed PS-b-P4VP having various total molecular weights (MWs) with $V_{PS}/V_{P4VP}$ close to 1.87 (Table 2-1) and followed the same procedure for creation of patchy micelles. All of them showed the micelles having three patches (Figure 2-7), implying that $V_{PS}/V_{P4VP}$ can be considered as a key factor for the number of patches per micelle during the patch formation. This observation also indicates that the patch size is controllable by varying the total MW with keeping the same $V_{PS}/V_{P4VP}$ (Figures 2-6 and 2-7). A theoretical study will provide better understanding on the patch formation and will be pursued. It is noted that micelles having more than three patches were hardly observed, although we found a micelle having four patches in a tetrahedral shape but did not have enough evidences yet.

In the case of PS-b-P4VP having $V_{PS}/V_{P4VP}$ higher than 2.0, micelles had two patches after the procedure for patch formation with a wide range of total MWs from 24 kg/mol to 100 kg/mol. The information including TEM images for two patch cases are given in figures and tables (Table 2-1, Figure 2-7). A representative example of micelles having two patches is shown in Figure 1b with PS(51k)-b-P4VP(18k) which has $V_{PS}/V_{P4VP}$ of 3.10. It is noted that spherical micelles of PS(51k)-b-P4VP(18k) before patch formation showed a similar diameter of 59.4 nm (±4.5 nm) to that of PS(41k)-b-P4VP(24k) micelles (Figure 2-5).

In Figure 2-1(b), two dark spherical patches stained with $RuO_4$ were connected to the bright P4VP core which is discernible between two patches and clearly visible in the enlarged image of a single micelle (left inset). This direct exposure of the P4VP core to the solvent is important for linear assembly of patchy micelles because it can provide the lateral repulsion between micelles to avoid non-directional aggregation. We will come back to this discussion later. The P4VP core in spherical shape can be also found in the image stained with $I_2$ (right inset). The micellar radius (from the center to the one end of two patches) (~30.7 nm) is comparable to that (~31.6 nm) of the micelles with three patches, indicating that they are suitable for simultaneous incorporation into a suparacolloidal chain with respect to the size. The patch radius (~15.2 nm) in two patches is slightly larger than that (~14.1 nm) in three patches. This slight difference in the patch size will make the reactivity of two patches greater than that of three patches when they are connected into a supracolloidal chain. We can find a few micelles having asymmetric two patches and some dimerized micelles with connected patches in Figure 1b. It is noted that micelles having three patches (1.0 %, 10 micelles when 1000 micelles counted) were also formed together with micelles with two patches.

We note that the corona seemed to be divided into several tiny patches with $V_{PS}/V_{P4VP}$ lower than 1.5. However, they were not clearly discernible in TEM images so that we do not have enough evidences of patchy formation in this case.

We investigated the effect of solvent quality on the formation of patchy

micelles with the solubility parameter δ as a probing factor for preference of a solvent to each block. Based on the δ values (unit of $MPa^{1/2}$), toluene (18.2) is a good solvent for PS (18.6) but a non-solvent for P4VP (22.2) so that a spherical micelle consisting of the PS corona and the P4VP core formed in toluene. By adding 1,4-dioxane (20.5), which has a slightly larger δ than toluene, into a toluene solution of micelles, spherical micelles remained, regardless of the amount of 1,4-dioaxane (Table 2-2). However, by the addition of DMF (24.8), which is a good solvent for P4VP but a poor solvent for PS, patchy micelles were obtained above ~65 wt% DMF by rearranging the PS corona into segregated patches with the central P4VP directly exposed to DMF. Patchy micelles were also produced with a polar solvent having δ close to that of DMF such as DMAc (22.7), γ-butyrolactone (26.3), and DMSO (26.7). TEM images of observed micelles are summarized in Supporting Information (Table 2-2). In the same solvent quality, micelles of PS(51k)-b-P4VP(18k) and PS(41k)-b-P4VP(24k) generated two and three patches, respectively. We note that precipitation was observed in high contents of γ-butyrolactone and DMSO, presumably because the PS block became insoluble. It is noted that the crosslinked P4VP would have a higher δ than that of pure P4VP due to ionic charges by the crosslinking agent.

We summarized the number of patches per micelle depending on the total MW and $V_{PS}/V_{P4VP}$ in Figure 2-2. Micelles having two patches were formed with $V_{PS}/V_{P4VP}$ above 2.0 and up to 4.5 within our experimental selections when the total MW was relatively low. In the case of high total MWs, however, two

patches were created only with $V_{PS}/V_{P4VP}$ below 3.5, indicating that the PS corona cannot be segregated into separated patches because of a large amount of the PS corona having a high MW. In contrast, three patches per micelle were produced with a narrow range of $V_{PS}/V_{P4VP}$ (1.5~2.0) in our selections of PS-b-P4VP. Within the results, however, the highest total MW for three patches is almost double of the lowest total MW so that the patch size as well as the micelle size can be controlled as long as keeping the similar $V_{PS}/V_{P4VP}$ (Figure 2-6). In the cases of high $V_{PS}/V_{P4VP}$ with high total MWs (marked by the bright cross in Figure 2-2), the small core compared to the corona was positioned close to the surface of the micelle instead of creating separated patches upon the same process for patch formation. The large core compared to the corona (marked by the dark cross in Figure 2-2) was also moved close to the surface of the micelle without patch formation. We are currently investigating morphological changes in micelles for these cases.

As we emphasized at the beginning, production of a regular micelle with three patches is a critical step to demonstrate a supracolloidal chain having controlled branches and an ultimately crosslinked supracolloidal network. We will first show a linear supracolloidal chain without a branch by using only micelles with two patches. When water is added to a solution of patchy micelles of PS-b-P4VP, the non-polar PS patch becomes unfavorable to the contact with water so that attraction between the PS patches of neighboring micelles is exerted, leading to the polymerization of patchy micelles. Thus, the PS patch can be considered as a

functional group in the reaction. In contrast, the central P4VP core, which is polar and exposed to the solvent, is not directly involved in the reaction between neighboring micelles. However, it is also essential for the polymerization of patchy micelles because it provides lateral repulsion between the patchy micelles to avoid non-directional aggregation. [10,22] In other words, patchy micelles would be uncontrollably aggregated if they do not have the part favorable to the solvent during the polymerization initiated by addition of the unfavorable solvent for the patches. Therefore, the micelle with two patches can be regarded as a bifunctional nano-building block or colloidal monomer represented by ARA or $RA^2$, where A and R indicate a functional group and a central unit, respectively, an analogue to a monomer in a conventional step-growth polymerization.

We polymerized bifunctional micelles of PS(51k)-b-P4VP(18k) into supracolloidal chains. Figure 2-3(a) shows the chains polymerized for 24 h. All of them are linear without particular branches and look undulated along the chain direction. In the enlarged image of the inset of Figure 2-3(a), we can identify the undulation coming from an alternating structure of combined two PS patches and the exposed P4VP core, in which PS parts were selectively stained with $RuO_4$ and appeared dark. Since two patches from the neighboring micellar monomers were combined in the chain, the volume of the PS unit was doubled, compared to the single patch in the micellar monomer, which can be distinguished as the small chain end, i.e., an unreacted patch, in the enlarged image. Because of the unfavorable contact with water, the dark PS unit became close to a spherical shape

in the chain to reduce the surface energy. The linear chain structure having alternating plump PS and exposed P4VP with two small chains ends was also discernible by scanning electron microscopy (Figure 2-8). The chains in Figure 3a show a length distribution, i.e., a distribution of the degree of polymerization (DP) because the supracolloidal polymerization is step-growth of bifunctional micelles. The average DP of 12 chains in Figure 2-1(a) is 26.3. We estimated the extent of reaction of the patches as 0.962 by counting 24 unreacted patches (chain ends) and 632 reacted patches (double of the monomer units in all chains) in Figure 2-1(a). To verify a step-growth polymerization of bifunctional micelles, a study on the kinetics and statistics on supracolloidal polymerization with much more chains than those in Figure 2-3(a) is necessary and currently in progress. It is noted that crossing of two chains with physical overlapping can be found in Figure 2-3(a). We also note that a kink in the chain shown in the left side of Figure 2-3(a) is the unit from a micelle with three patches which was unavoidably formed with micelles having two patches. We here emphasize that we hardly observed braches in linear supracolloidal chains when we analyzed chains in larger areas than the image of Figure 2-3(a). We note that 12.5 wt% water was mostly added for supracolloidal polymerization. Chains were also induced by the addition of 10~30 wt% water (Figure 2-8). However, precipitation was observed with a large amount of water (> 30 wt%) and polymerization was not induced with a small amount of water (< 10 wt%). By adding 12.5 wt% methanol ($\delta$ = 29.6 $MPa^{1/2}$) or ethylene glycol ($\delta$ = 33.0 $MPa^{1/2}$), instead of water ($\delta$ = 47.8 $MPa^{1/2}$),

polymerization of patchy micelles was also initiated (Figure 2-9). The uniform size of bifunctional colloidal monomers of PS(51k)-b-P4VP(18k) is primarily responsible for a linear chain without a branch. If building blocks have a broad size distribution, an arbitrary connection with more than two building blocks, which can be a branching point, could be frequently produced

To introduce branches in supracolloidal chains, we polymerized bifunctional micelles of PS(51k)-b-P4VP(18k) with 5.0 % PS(41k)-b-P4VP(24k) micelles having three patches for the same period of 24 h as in the previous case. The micelle with three patches can be regarded as a trifunctional colloidal monomer of $RA^3$. According to the Carothers gelation theory, the average functionality ($f_{av}$) per colloidal monomer in this case is 2.05 (2×0.95 + 3×0.05) and the gel point ($p_c = 2 / f_{av}$) is 0.975. Thus, we can expect branching without gelation until the extent of reaction reaches to a full conversion. As shown in Figure 2-3(b), nonlinear supracolloidal chains were successfully polymerized with the addition of trifunctional micelles. The chains were forked at the branching units of the micelles having three patches. Branching was created only at the trifunctional micelle. In the enlarged image (right inset) of Figure 2-3(b), we can clearly find the branching point marked by the arrow. We note that there are physical crossings of two chains. We estimated the extent of reaction of the patches as 0.933 by counting 55 unreacted patches and 819 reacted patches in Figure 2-1(b). This value is lower than the theoretical gel point of 0.975. We note that all of the trifunctional units incorporated in the chains did not make the

branches. As shown in the left inset of Figure 2-3(b), the trifunctional units were inserted in the middle of the chain and also at the end of the chain without further reactions. It is noted that the amount of trifunctional units in the entire chains shown in Figure 2-3(b) was about 3.7 % (15 micelles out of 402 micelles), which is smaller than that added initially (5.0 %). As we mentioned earlier, the patch radius (~14.1 nm) in the trifunctional micelle is slightly smaller than that (~15.2 nm) in the bifunctional micelle. Thus, the trifunctional patches of the non-polar PS can be more tolerant to the addition of water than the bifunctional patches due to their smaller size. In other words, a smaller patch implies less reactive toward the combining reaction between two patches to avoid unfavorable contact with water. The unreacted patches of trifunctional units in the chains can be understood with the lower reactivity of the trifunctional patches.

We further polymerized linear and branched supracolloidal chains shown in Figure 2-3 for additional 24 h (total 48 h). Since the extent of reaction for combining patches was closed to a full conversion in this condition, dramatic difference between the polymerization only with bifunctional micelles and that by adding trifunctional micelles was observed, that is, long linear chains (Figure 4a) versus crosslinked chains (Figure 2-4(b)). Figure 2-4(a) shows a representative linear supracolloidal chain having the DP of 205. Several chains with various DPs are given in Figure 2-10. The chains became much longer than those shown in Figure 2-3(a) but they are still linear without branches. We can understand the high DP based on the Carother polymerization theory, in which

the average DP becomes very large close to a full conversion according to the simple equation of $1/(1 - p)$, where $p$ is the extent of reaction. With the average DP of 152 from 6 chains (Figures 2-4(a) and 2-10), $p$ is 0.993. We note that a solution of bifunctional micelles was very dilute (~1.4 nM by considering a single micelle as one molecule having a volume of ~1.07 × 105 $nm^3$ estimated from Figure 2-5). The dilute condition made the chains well separated on a TEM grid so that only a single chain was independently imaged in a reasonable magnitude for visualizing a whole chain. It is noted that supracolloidal polymerization of bifunctional micelles apparently followed the kinetics of catalyzed step-growth polymerization, i.e., a linear increase of the size with respect to the polymerization time, when dynamic light scattering measurements were employed (Figure 2-11). To confirm the kinetics, however, precise analysis on time-dependent DPs of chains in TEM images is necessary. In sharp contrast, we obtained crosslinked supracolloidal chains, a network structure, by the addition of 5.0 % trifunctional micelles as shown in Figure 2-4(b). All chains were incorporated into the network so that an independent chain was hardly observed. In the left inset of Figure 2-4(b), we can clearly find the chain connected between two junctions of trifunctional micelles. The network formation can be also understood by the Carothers gelation theory because the condition here ($p > 0.99$ based on the case of linear chains) was above the gel point ($p_c = 0.975$). We note that there are many physical overlaps of chains, which are not easily differentiated from trifunctional units in a low magnitude image of Figure 2-4(b). An enlarged

image of physically overlapped parts is given in the middle inset for comparison, which shows the overlapped part distinguished from the crosslinked unit. It is noted that a dangling chain end can be also found as shown in the right inset of Figure 2-4(b). We did not observe gelation of an entire solution because of a very low concentration of the solution. Instead, we found several independent networks on the same TEM grid. Increasing a solution concentration as well as an amount of trifunctional micelles is one of our on-going research topics.

## 2-4. Conclusion

In summary, we successfully demonstrated controlled branching and eventual crosslinking in supracolloidal chains by introducing well-defined trifunctional patchy micelles. Three patches in the micelles worked as the distinct parts for crosslinking as well as branching, analogues to multifunctional groups in classical gelation of small molecular monomers. These branched and crosslinked supracolloidal chains were well compared with long linear chains only with bifunctional micelles. We were able to understand the formation of linear chains and networks of patchy micelles by the classical theory of polymerization and gelation. Furthermore, we delivered real visual images on branching and crosslinking in chain-like structures which cannot be directly imaged in conventional gelation of small multifunctional monomers. Branched and crosslinked supracolloidal chains can find potential uses in similar areas for small molecular branches and networks such as elastomeric gels and scaffold applications. Moreover, various functional nanomaterials can be incorporated into the micellar units of supracolloidal structures to deliver customized functionalities to the networks.

## 2-5. References


[1] Li, F.; Josephson, D. P.; Stein, A. Angew. Chem. Int. Ed. **2011**, 50, 360.

[2] Duguet, E.; Desert, A.; Perro, A.; Ravaine, S. Chem. Soc. Rev. **2011**, 40, 941.

[3] Sacanna, S.; Pine, D. J. Curr. Opin. Colloid Interface Sci. **2011**, 16, 96.

[4] Teulle, A.; Bosman, M.; Girard, C.; Gurunatha, K. L.; Li, M.; Mann, S.; Dujardin, E. Nat. Mater. 2015, 14, 87.

[5] Schreiber, A.; Huber, M. C.; Colfen, H.; Schiller, S. M. Nat. Commun. 20**1**5, 6, 6705.

[6] Pavlopoulos, N. G.; Dubose, J. T.; Pinna, N.; Willinger, M. G.; Char, K.; Pyun, J. Angew. Chem. Int. Ed. **2016**, 55, 1787.

[7] Demirors, A. F.; Pillai, P. P.; Kowalczyk, B.; Grzybowski, B. A. Nature **2013**, 503, 99.

[8] Walther, A.; Müller, A. H. E. Chem. Rev. **2013**, 113, 5194.

[9] Gröschel, A. H.; Schacher, F. H.; Schmalz, H.; Borisov, O. V.; Zhulina, E. B.; Walther, A.; Müller, A. H. E. Nat. Commun. **2012**, 3, 710.

[10] Gröschel, A. H.; Walther, A.; Löbling, T. I.; Schacher, F. H.; Schmalz, H.; Müller, A. H. E. Nature **2013**, 503, 247.

[11] Cui, H.; Chen, Z.; Zhong, S.; Wooley, K. L.; Pochan D. J. Science **2007**, 317,

617.

[12] Tang, Z.; Kotov, N. A.; Giersig, M. Science **2002**, 297, 237.

[13] Hill, L. J.; Richey, N. E.; Sung, Y.; Dirlam, P. T.; Griebel, J. J.; Lavoie-Higgins, E.; Shim, I.; Pinna, N.; Willinger, M.; Vogel, W.; Benkoski, J. J.; Char, K.; Pyun, J. ACS nano **2014**, 8, 3272.

[14] Zhang, K.; Jiang, M.; Chen, D. Prog. Polym. Sci. **2012**, 37, 445.

[15] Choueiri, R. M.; Klinkova, A.; Therien-Aubin, H.; Rubinstein, M.; Kumacheva, E. J. Am. Chem. Soc. **2013**, 135, 10262.

[16] Lai, J.; Xu, Y.; Mu, X.; Wu, X.; Li, C.; Zheng, J.; Wu, C.; Chen, J.; Zhao, Y. Chem. Commun. **2011**, 47, 3822.

[17] Wang, H.; Chen, L.; Shen, X.; Zhu, L.; He, J.; Chen, H. Angew. Chem. Int. Ed. **2012**, 51, 8021.

[18] Du, J.; O'Reilly, R. K. Chem. Soc. Rev. **2011**, 40, 2402.

[19] Lunn, D. J.; Finnegan, J. R.; Manners, I. Chem. Sci. **2015**, 6, 3663.

[20] Gröschel, A. H.; Müller, A. H. E. Nanoscale **2015**, 7, 11841.

[21] Hill, L. J.; Pinna, N.; Char, K.; Pyun, J. Prog. Polym. Sci. **2015**, 40, 85.

[22] Nie, Z.; Fava, D.; Kumacheva, E.; Zou, S.; Walker, G. C.; Rubinstein, M. Nat. Mater. **2007**, 6, 609.

[23] Kim, J. H.; Kwon, W. J.; Sohn, B. H. Chem. Commun. **2015**, 51, 3324.

[24] Chae, S.; Lee, S.; Kim, K.; Jang, S. W.; Sohn, B. H. Chem. Commun. **2016**, 52, 6475.

[25] Flory, P. J. Principles of Polymer Chemistry (Cornell Univ. Press, New York, **1953**).

[26] Li, M.; Johnson, S.; Guo, H.; Dujardin, E.; Mann, S. Adv. Funct. Mater. **2011**, 21, 851.

[27] Liu, K.; Nie, Z.; Zhao, N.; Li, W.; Rubinstein, M.; Kumacheva, E. Science, **2010**, 329, 197.

[28] Fang, B.; Walther, A.; Wolf, A.; Xu, Y.; Yuan, J.; Muller, A. H. E. Angew. Chem. Int. Ed., **2009**, 48, 2877.

[29] Wang, Y.; Wang, Y.; Breed, D. R.; Manoharan, V. N.; Feng, L.; Hollingsworth, A. D.; Weck, M.; Pine, D. J. Nature **2012**, 491, 51.

[30] Liu, Y.; Liu, B.; Nie, Z. Nano Today **2015**, 10, 278.

[31] Vogel, N.; Retsch, M.; Fustin, C.; Campo, A. D.; Jonas, U. Chem. Rev. **2015**, 115, 6265.

[32] Ku, K. H.; Kim, Y.; Yi, G.; Jung, Y. S.; Kim, B. J. ACS Nano **2015**, 9, 11333.

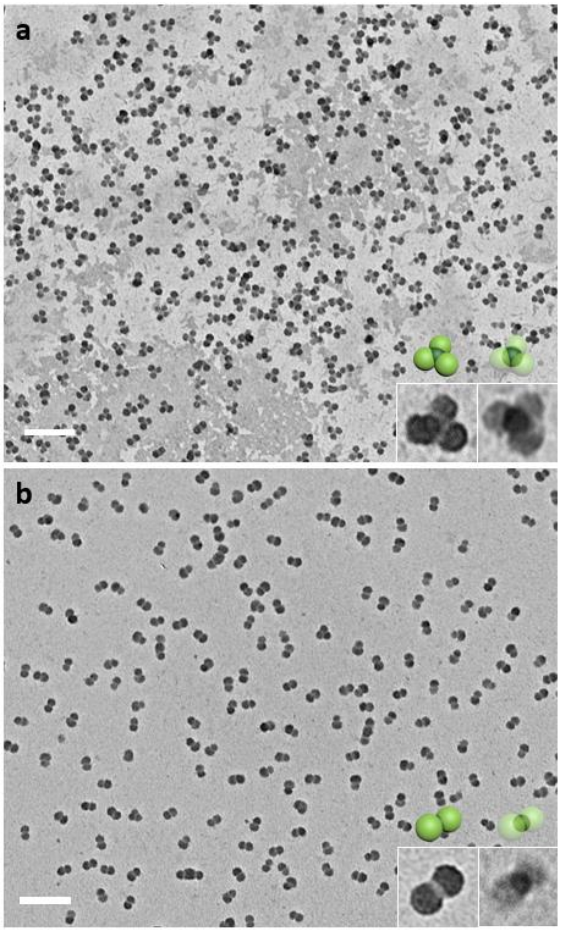


**Figure 2-1.** TEM images: (a) PS(41k)-*b*-P4VP(24k) micelles having three patches; (b) PS(51k)-*b*-P4VP(18k) micelles having two patches. The scale bars are 200 nm. Each inset is an enlarged image (80 nm × 80 nm) of an individual micelle. $RuO_4$ and $I_2$ stained the PS patches (left inset) and the P4VP core (right inset), respectively.

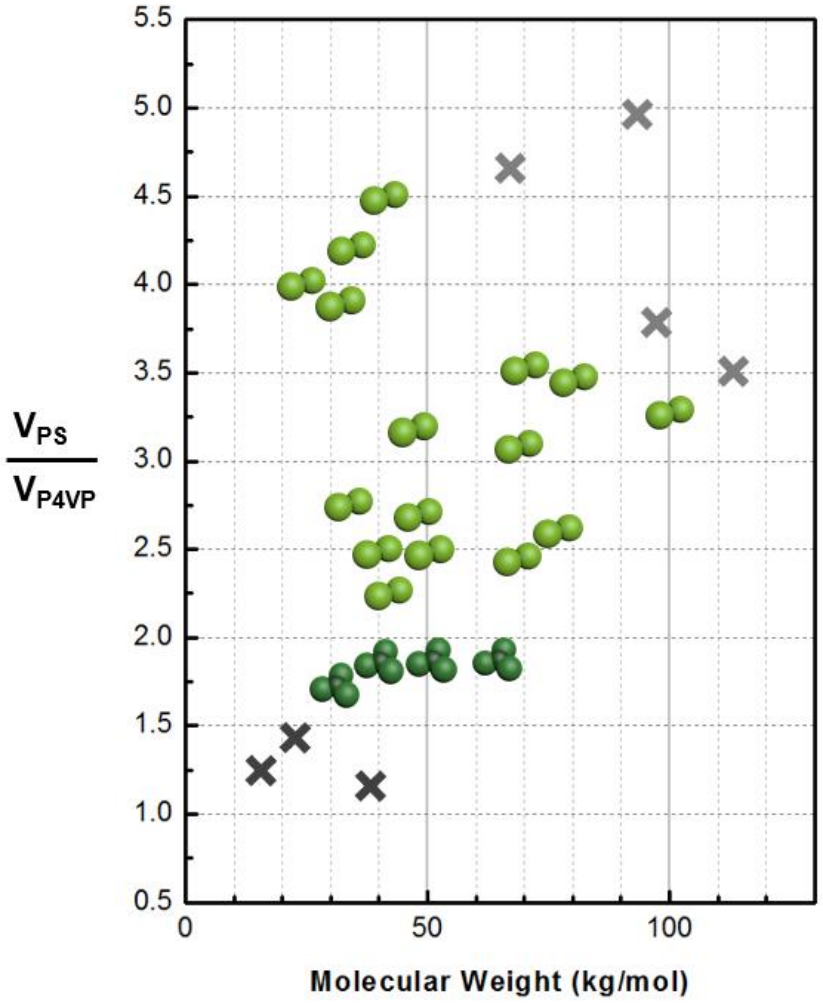


**Figure 2-2.** Micelles with two and three patches depending on the total molecular weight and the volume ratio of PS to P4VP.

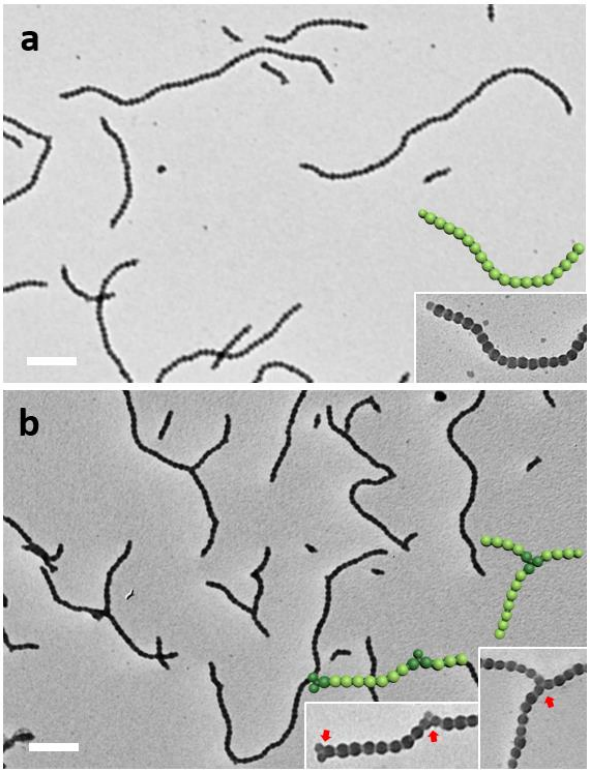


**Figure 2-3.** TEM images: (a) linear chains of bifunctional micelle; (b) branched chains by adding 5.0 % trifunctional micelles. The PS block was stained with $RuO_4$. The scales bars are 300 nm. All insets are 2-fold enlarged images. Trifunctional micelles in the insets are indicated by arrows.

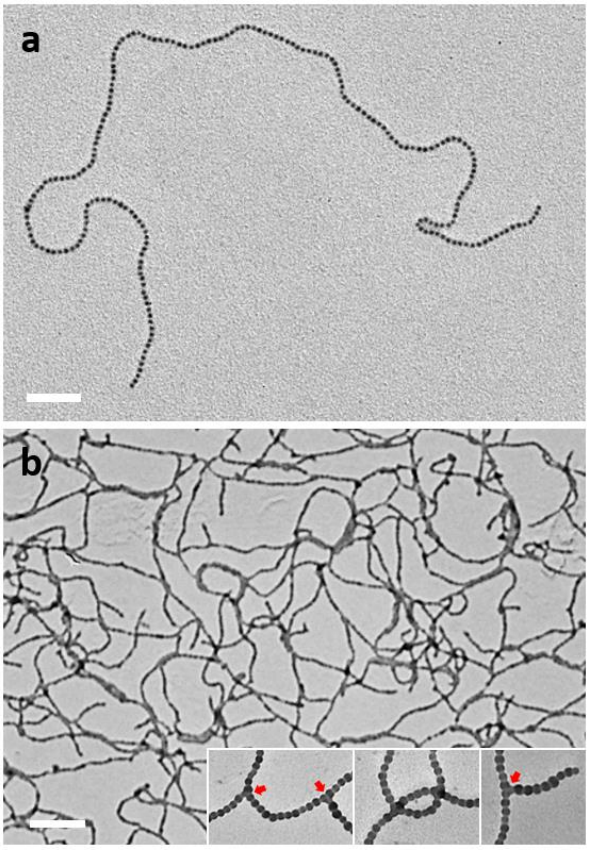


**Figure 2-4.** TEM images after 48 h supracolloidal polymerization: (a) a long linear chain of bifunctional micelles; (b) crosslinked chains by adding 5.0 % trifunctional micelles. The P4VP block was stained with $I_2$. The scales bars are 300 nm. The insets are 2-fold enlarged images stained with $RuO_4$. The arrows indicate trifunctional micelles.

| | $V_{PS}/V_{P4VP}$ | Patch Number |
|---|---|---|
| PS(20k)-*b*-P4VP(19k) | 1.15 | X |
| PS(10k)-*b*-P4VP(8k) | 1.31 | |
| PS(12k)-*b*-P4VP(10k) | 1.38 | |
| PS(21k)-*b*-P4VP(13k) | 1.77 | 3 |
| PS(41k)-*b*-P4VP(24k) | 1.87 | |
| PS(24k)-*b*-P4VP(14k) | 1.88 | |
| PS(31k)-*b*-P4VP(18k) | 1.89 | |
| PS(29k)-*b*-P4VP(14k) | 2.27 | 2 |
| PS(34k)-*b*-P4VP(15k) | 2.48 | |
| PS(48k)-*b*-P4VP(21k) | 2.49 | |
| PS(30k)-*b*-P4VP(13k) | 2.53 | |
| PS(52k)-*b*-P4VP(22k) | 2.59 | |
| PS(32k)-*b*-P4VP(13k) | 2.65 | |
| PS(24k)-*b*-P4VP(10k) | 2.77 | |
| PS(51k)-*b*-P4VP(18k) | 3.10 | |
| PS(35k)-*b*-P4VP(12k) | 3.19 | |
| PS(75k)-*b*-P4VP(25k) | 3.29 | |
| PS(59k)-*b*-P4VP(19k) | 3.48 | |
| PS(53k)-*b*-P4VP(17k) | 3.52 | |
| PS(25k)-*b*-P4VP(7k) | 3.91 | |
| PS(19k)-*b*-P4VP(5k) | 4.00 | |
| PS(27k)-*b*-P4VP(7k) | 4.22 | |
| PS(33k)-*b*-P4VP(8k) | 4.50 | |
| PS(87k)-*b*-P4VP(27k) | 3.53 | X |
| PS(76k)-*b*-P4VP(22k) | 3.78 | |
| PS(55k)-*b*-P4VP(13k) | 4.63 | |
| PS(77k)-*b*-P4VP(17k) | 4.96 | |

**Table 2-1.** List of PS-*b*-P4VP with volume ratios of PS to P4VP and patch numbers. The number in the parentheses is a molecular weight in g/mol.

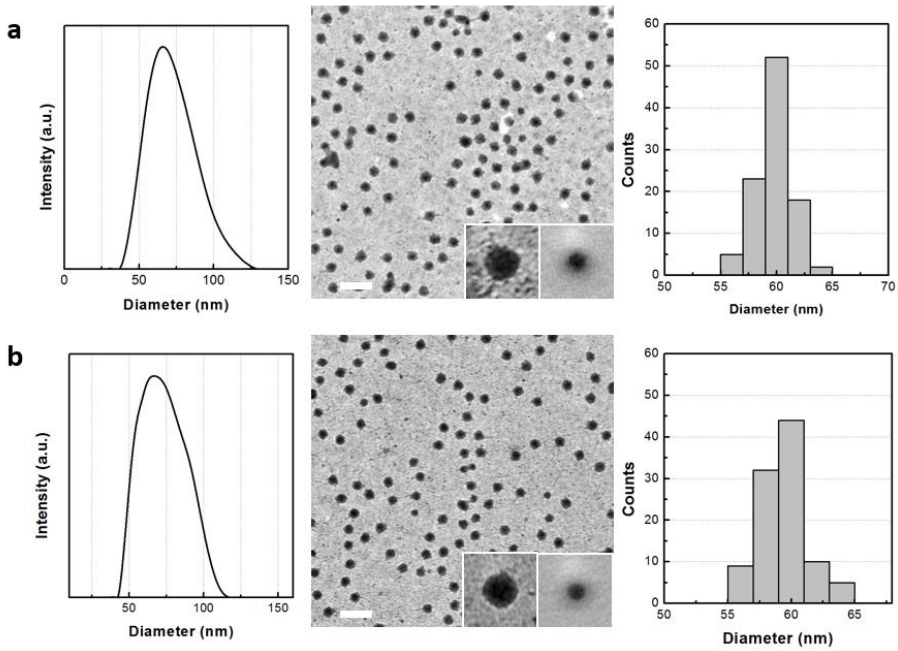


**Figure 2-5.** Spherical micelles of (a) PS(41k)-*b*-P4VP(24k) and (b) PS(51k)-*b*-P4VP(18k): (left column) diameter distributions by DLS; (center column) TEM images after $RuO_4$ staining; (right column) diameter histograms from TEM images. The scale bars in the TEM images are 200 nm. The insets are enlarged images (100 nm × 100 nm) of micelles stained with $RuO_4$ (left) and $I_2$ (right).

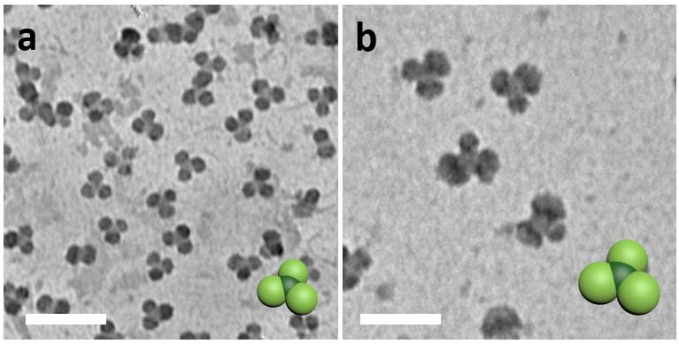


**Figure 2-6.** TEM images of small and large micelles having three patches: (a) PS(21k)-*b*-P4VP(13k); (b) PS(41k)-*b*-P4VP(24k). PS patches were stained with $RuO_4$. The scale bars are 100 nm.

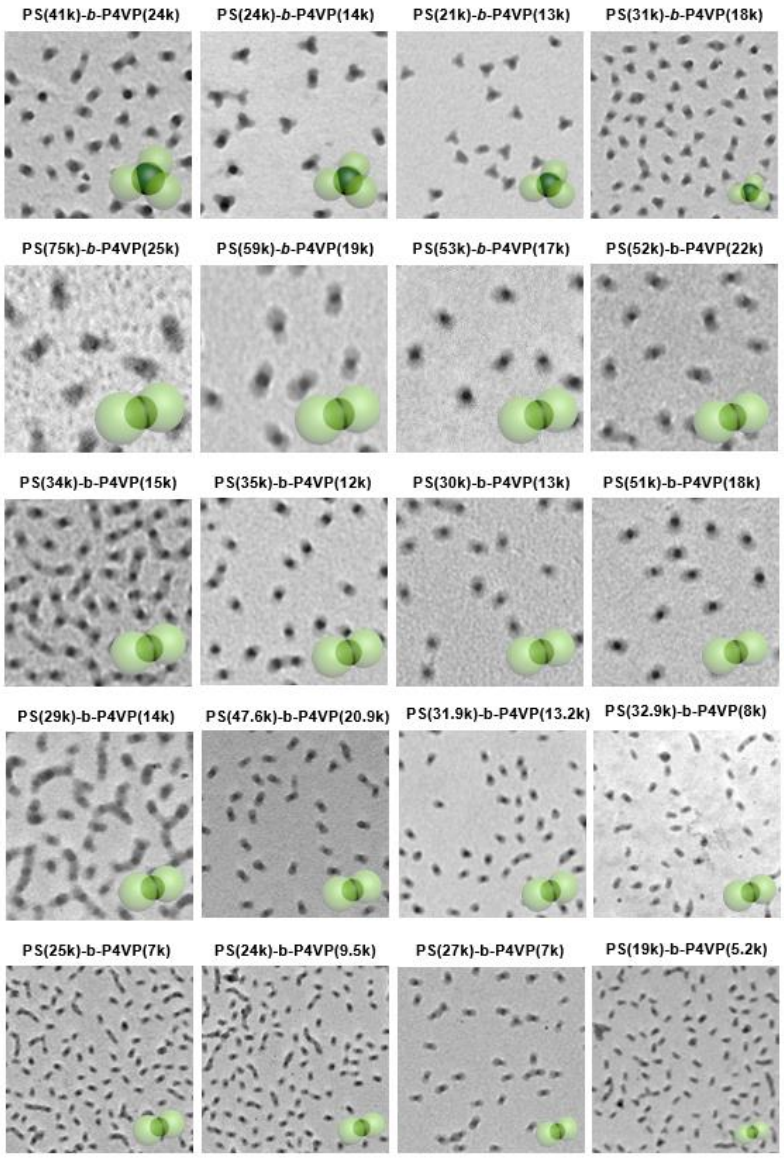


**Figure 2-7.** TEM images of micelles having two and three patches. The size of each image is 450 nm × 450 nm. P4VP cores were stained with $I_2$.

| Solvent | 1,4-Dioxane | | DMAc (N,N-Dimethylacetamide) | | DMF (N,N-Dimethylformamide) | | γ-Butyrolactone | | DMSO (Dimethylsulfoxide) | |
|---|---|---|---|---|---|---|---|---|---|---|
| δ ($MPa^{1/2}$) | 20.5 | | 22.7 | | 24.8 | | 26.3 | | 26.7 | |
| 50 wt% |  |  |  |  |  |  |  |  |  |  |
| 67 wt% |  |  |  |  |  |  |  |  |  |  |
| 80 wt% |  |  |  |  |  |  |  |  |  |  |
| 89 wt% |  |  |  |  |  |  |  |  | *precipitated* | |
| 99 wt% |  |  |  |  |  |  | *precipitated* | | *precipitated* | |

**Table 2-2.** Micelles of PS(51k)-*b*-P4VP(18k) (left) and PS(41k)-*b*-P4VP(24k) (right) in toluene mixed with polar solvents having various solubility parameters (δs). The size of each TEM image is 80 nm × 80 nm. Micelles were stained with $RuO_4$. Each polar solvent was added to a 0.1 wt% toluene solution (0.1 g) of crosslinked micelles by a syringe pump at a rate of 50 ml/h.

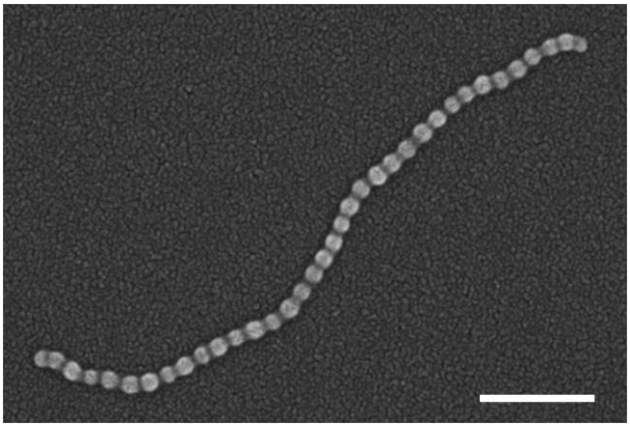

**Figure 2-8.** SEM image of a linear supracolloidal chain of PS(51k)-*b*-P4VP(18k). The scale bar is 200 nm.

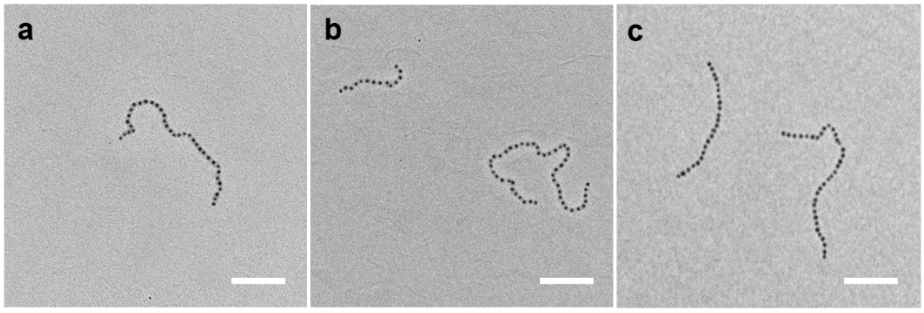


**Figure 2-8.** TEM images after 12 h supracolloidal polymerization of patchy micelles of PS(51k)-*b*-P4VP(18k) by adding different amounts of water: (a) 12.5 wt%; (b) 20.0 wt%; (c) 27.5 wt%. The P4VP block was stained with $I_2$. The scales bars are 300 nm.

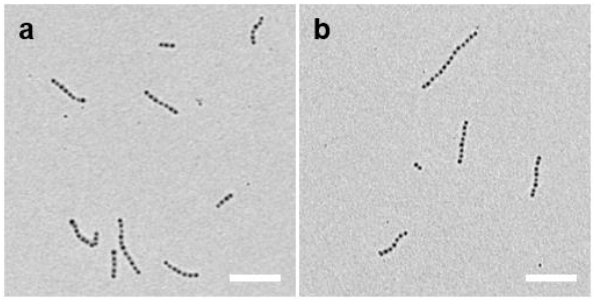


**Figure 2-9.** TEM image after 12 h supracolloidal polymerization of patchy micelles of PS(51k)-b-P4VP(18k) by adding 12.5 wt% polar solvent instead of water: (a) methanol; (b) ethylene glycol. The P4VP block was stained with $I_2$. The scales bars are 300 nm.

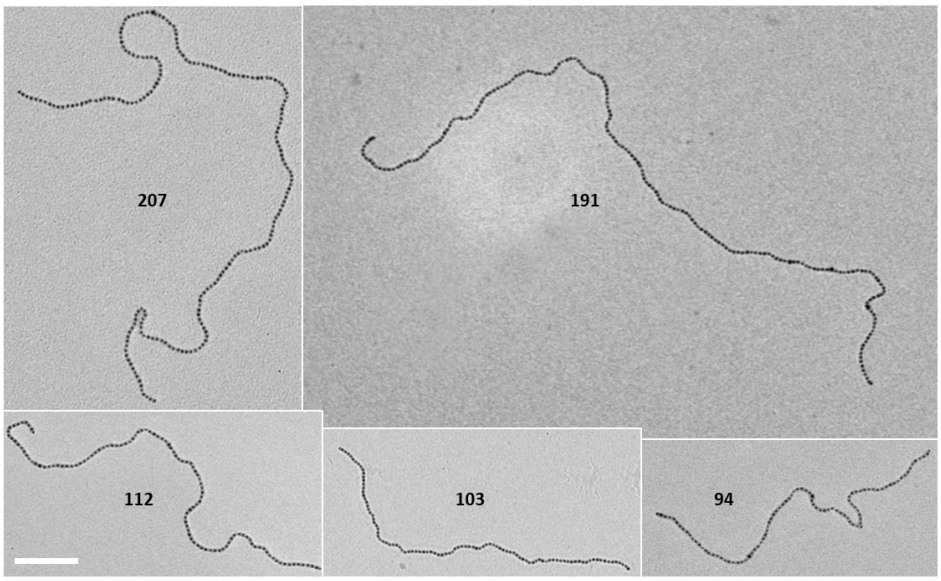


**Figure 2-10.** TEM images of long linear supracolloidal chains of bifunctional micelles with various DPs. The number with each chain is the DP of the chain. The scale bar is 500 nm.

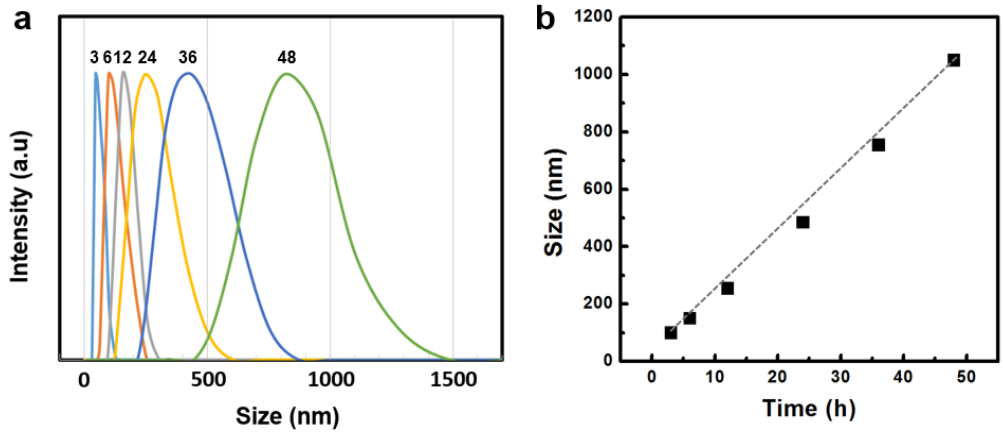


**Figure 2-11.** (a) Size distributions of supracolloidal chains of bifunctional micelles of PS(51k)-*b*-P4VP(18k) after various polymerization hours; (b) Linear dependence of the size on the polymerization time.

# Chapter 3.

# Diblock Copolymer Micelles as Surface-Functionalized Particles and Direct Decoration of Nanoparticles on Their Surface

## 3-1. Introduction

Dielectric particles coated by metallic shells or nanoparticles have been widely investigated for catalytic [1] and optical applications [2], including surface enhanced Raman scattering [3] and photonic crystals [4]. Silica particles synthesized by the sol-gel process are one of the most popular templates for decoration of shells and nanoparticles because their sizes are well-controllable in addition to their chemical and mechanical stability [5]. To attach metallic or inorganic nanoparticles on silica particles, however, modification of their surface by silane compounds or charged polymers is compulsory [6,7].

Polymeric particles are also commonly employed for spherical templates to be decorated by nanoparticles [8]. Compared to silica particles, one of the main advantages of polymeric particles is favorable dispersion in aqueous media due to relatively low densities of polymeric materials. Polystyrene (PS) particles synthesized by the classical emulsion polymerization are largely used for such purpose [9]. However, surface modification is essential to attach nanoparticles on PS particles. For example, the surface of PS particles can be directly sulfonated and then nanoparticles can be adsorbed on the sulfonated PS particles [10]. Surface functionalization can be also achieved by adding co-monomers of acrylic acid during the synthesis of PS particles, which provides functional groups of carboxylates on the surface of PS particles [11]. For effective attachment of

nanoparticles, however, further modification of carboxylate-functionalized PS particles was performed by the reaction with thiol-functional molecules [12] or by layer-by-layer adsorptions of polyelectrolytes [13].

Since the surface area per volume increases with the decrease of the particle size, larger amounts of nanoparticles can be utilized if smaller particles are adopted as templates for decoration of nanoparticles. Since typical synthetic methods of silica and PS particles provide particles with the diameters larger than 100 nm [9], it requires great efforts to synthesize particles with the diameters smaller than 100 nm. In contrast, spherical micelles of diblock copolymers generally have the diameters in the range of 10 to 100 nm [14]. Thus, they can be a potential candidate of smaller template particles for decoration of nanoparticles, compared to usual silica or PS particles

In an aqueous solution, amphiphilic diblock copolymers form spherical micelles consisting of soluble hydrophilic coronas and insoluble hydrophobic cores [14]. A conventional usage of copolymer micelles is to solubilize otherwise insoluble substances such as drugs [15], dyes [16], and quantum dots [17] by encapsulating them in the cores. However, we will apply micelles of diblock copolymers to effective template particles with the diameter smaller than 100 nm to produce particles decorated with nanoparticles.

In this study, we first synthesized diblock copolymers of the PS block and the block containing activated esters by the reversible addition fragmentation chain

transfer (RAFT) polymerization. Since activated esters can efficiently react with amine groups [18], we then replaced the activated ester with dopamine functionality, resulting in diblock copolymers consisting of the PS block and the dopamine-functionalized block. We selected the dopamine functionality because it can strongly bind to the surface of metal oxides and can reduce metal ions without reducing agents [19]. By dissolving this amphiphilic diblock copolymer in water, spherical micelles of ~40 nm in diameter were induced. Since these micelles have the PS cores with the dopamine-functionalized coronas, they can be considered as PS particles with dopamine-functionalized surface. Thus, without additional surface functionalization, we successfully decorated the PS particles, originated from the copolymer micelles, with Ag and $TiO_2$ nanoparticles due to the dopamine functionality on the surface of PS particles.

## 3-2. Experimental Section

*Materials*

All chemicals were commercially available and used as received unless otherwise stated. 2.2'-Azoisobutyronitrile (AIBN) was recrystallized from diethylether. All solvents were purified by common procedures.

*Synthesis of Pentafluorophenyl acrylate (PFPA)*

PFPA monomers were synthesized as described in the literature [18]. In a round bottom flask equipped with a dropping funnel and a magnetic stir bar, pentafluorophenol (17.1 mL, 0.16 mol) was dissolved in anhydrous dichloromethane (200 mL) under nitrogen atmosphere. Triethylamine (27.3 mL, 0.19 mol) was added via syringe through a septum. The dropping funnel was filled with acryloyl chloride (16.5 mL, 0.19 mol) under nitrogen atmosphere and this component was then dropped slowly to the reaction mixture while stirring vigorously and cooling with an ice bath. After complete addition, the reaction mixture was cooled for 30 min and then slowly warmed to room temperature for overnight. It was extracted with water (200 mL) three times. The organic phase was dried over $MgSO_4$, concentrated by rotary evaporation and subsequently

vacuum distilled. Pentafluorophenyl acrylate was isolated at 49℃ ($9.8 \times 10^{-2}$ mbar) as a colorless liquid (19.43 g, 0.077 mol, 71%).

$^{1}$H-NMR ($CDCl_3$, 300 MHz): δ [ppm] = 6.45 (m, 1H, C=$CH_2$-cis); 5.92 (m, 1H, C=$CH_2$-trans); 2.08 (s, 3H, -$CH_3$).

$^{19}$F-NMR ($CDCl_3$, 376 MHz): δ [ppm] = -152.74 (d, J = 19 Hz, 2F, o-ArF); -158.17 (t, J = 19 Hz, 1F, p-ArF); -162.45 (t, J = 19 Hz, 2F, m-ArF).

*Synthesis of Poly(pentafluorophenyl acrylate) (PPFPA)*

PPFPA was synthesized by the RAFT polymerization as shown in the literature [18]. For a typical procedure, a Schlenk tube equipped with a stir bar was loaded with pentafluorphenyl acrylate (PFPA) (15 g, 62.9 mmol), cumyl dithiobenzoate (272 mg, 0.99 mmol), and AIBN (23 mg, 0.14 mmol). All compounds were dissolved in anhydrous dioxane (2 mL). Following three freeze-pump-thaw cycles, the tube was immersed in an oil bath at 65℃ for about 24 h with vigorous stirring. The resulting polymer was isolated by precipitation in methanol. By re-dissolving the polymer in a few milliliters of THF, this process was repeated three times. The precipitated polymer was dried for 12 h at 23℃ under 10 mbar vacuum, providing P(PFPA) (9 g, 60%) as slightly pink powder. The number average molecular weight is 5,000 g/mol and polydispersity index is 1.1 by GPC

with PS standards.

*Synthesis of Poly(pentafluorophenyl acrylate)-b-Polystyrene (PPFPA-b-PS)*

To synthesize PPFPA-b-PS diblock copolymer, 1.12g (0.22 mmol, 1 eq.) of the PPFPA macro chain transfer agent and 3.6 mg (0.022 mmol, 0.1 eq.) AIBN, and styrene monomer (10 g) were added together with 3 mL THF in a Schlenk tube. Oxygen was exchanged by nitrogen after three freeze–pump–thaw cycles and then polymerization was carried out at 65℃ for 24 h. The block copolymer was purified by precipitation in methanol three times, resulting in 5.8 g (58%) of the reactive block copolymer. To remove PS homopolymer, Soxhlet extraction was performed with cyclohexane for 24 h. The number average molecular weight is 66,800 g/mol and polydispersity index is 1.08 by GPC with PS standards. The block ratio between PPFPA and PS was 1:14 by NMR.

$^1$H NMR (500 MHz, $CDCl_3$): δ [ppm]: 7.06 (m, 3 H, Ph-H), 6.57 (m, 2 H, Ph-H), 3.04 (m, 1 H, $CH_2$–CH–), 2.38 (m, 1 H, CH–$CH_2$), 1.87 (m, 1 H,CH–$CH_2$), 1.84 (m, 1 H), 1.39 (m, 2 H).

*Synthesis of Poly(dopamine acrylamide)-b-Polystyrene (PDA-b-PS)*

To modify the activated ester, post-polymerization modification was carried

out. PPFPA-b-PS (300 mg, 0.004 mmol, 1 eq.), dopamine hydrochloride (217 mg, 1.1 mmol, 15 eq.), and triethylamine (116 mg, 1.1 mmol, 15 eq.) were dissolved in a mixture of 2 mL of THF and 2 mL of DMF and stirred under nitrogen at room temperature for 12 h. Then, the solution was filtered and precipitated in methanol three times, yielding 240 mg (80%) of the product.

$^{1}$H NMR (500 MHz, $CDCl_3$ : MeOD = 4 : 1): δ [ppm]: 7.06 (m, 3 H, Ph-H), 6.57 (m, 2 H, Ph-H), 6.20 (m, 3 H, Ar-H dopamine), 3.52 (m, 2 H,CONH–$CH_2$–$CH_2$–Ph), 3.39 (m, 2 H, CONH–$CH_2$–$CH_2$–Ph), 2.97 (m, 1 H, $CH_2$–CH–), 2.38 (m, 1 H, CH–$CH_2$), 1.87 (m, 1 H,CH–$CH_2$), 1.84 (m, 1 H), 1.39 (m, 2 H).

$^{19}$F NMR (400 MHz,$CDCl_3$): no signals.

IR: max [cm-1]: 3374 (OHdopamine), 3027 (CH), 2923 (CH), 1650 (CONH).

*Synthesis of TiO2 nanoparticles*

$TiO_2$ nanoparticles were synthesized as described in the literature [19]. 1.25 mL of titanium tetraisopropoxide (TTIP) was dissolved in 25 mL of ethanol. This ethanol solution of TTIP was added to 250 mL of distilled water adjusted to pH 1.5 with nitric acid in drops at 4℃ with vigorous stirring. The mixture solution was further stirred overnight at room temperature and then $TiO_2$ nanoparticles were obtained by evaporating the liquid phase at 50℃.

*Fabrication of PDA-b-PS micelles*

0.1 mg of PDA-b-PS was dissolved in 0.1 mL of THF and then 1.0 mL of distilled water was added slowly to the solution with gentle stirring. After vigorous stirring for 30 min, THF from the solution was evaporated under reduced pressure. The remaining aqueous solution was filtered through a cellulose acetate membrane having 0.45 μm pores. The solution was stable for several months without any precipitation.

*Decoration of Ag nanoparticles on PDA-b-PS micelles*

10 mL of an aqueous solution of PDA-b-PS micelles was added to 20 mL of a freshly prepared $AgNO_3$ (0.12 M) aqueous solution. The mixture was stirred at room temperature for 30 min. The product was collected by filtering and was re-dispersed in ethanol for further characterization.

*Decoration of $TiO_2$ nanoparticles on PDA-b-PS micelles*

10 mL of an aqueous solution of PDA-b-PS micelles was added to 10 mL of an aqueous dispersion of $TiO_2$ nanoparticles. The mixture was stirred at room temperature for 12 h. The product was collected by filtering and was re-dispersed

in ethanol for further characterization..

*Characterizations*

NMR spectra were obtained on a Varian NMR System (500 MHz). Gel permeation chromatography (GPC) was carried out on a Waters system (1515 pump, 2414 refractive index detector) with a Shodex GPC LF-804 column. Transmission electron microscopy (TEM) was performed on a Hitachi 7600 operating at 100 kV. For scanning electron microscopy (SEM), a Hitachi 4300 operating at 15 kV was also used. UV-Vis absorption spectra were recorded on a Scinco S-3100 spectrophotometer. Dynamic light scattering (DLS) was carried out with an ALV/CGS-3 Compact Goniometer System.

## 3-3. Results and Discussion

To utilize diblock copolymer micelles for the fabrication of PS particles, we synthesized a diblock copolymer consisting of the PS block and the poly(pentafluorophenyl acrylate) (PPFPA) block which contains activated esters. The activate esters in the PPFPA block can be effectively substituted by functional molecules having primary amine groups [18]. The PPFPA block was first synthesized by the RAFT polymerization and then was used as a macro chain transfer agent for the polymerization of PPFPA-b-PS diblock copolymers (Figure 3-1). The number average molecular weight and polydispersity index of copolymers are 66,800 g/mol and 1.08, respectively. The molar ratio between PPFPA and PS is 1:14.

Dopamine is hydrophilic and can strongly bind to the surface of metal oxides. It can also adsorb and reduce metal ions. Thus, we covalently linked dopamine to PPFPA-b-PS copolymers by the reaction with activated esters in the PPFPA block, resulting in poly(dopamine acrylamide)-b-polystyrene, PDA-b-PS, as shown in Figure1.

By dispersing the synthesized PDA-b-PS copolymers in water, they organized into micelles with hydrophilic PDA coronas and hydrophobic PS cores, which have the average diameter of 45 nm by the dynamic light scattering (DLS)

analysis (Figure 3-2). We further characterized the shape and diameter of theses micelles by SEM and TEM as shown in Figure 3-3. Spherical particles are clearly visible in both SEM and TEM images. The average diameter of particles measured from the SEM image is 45 nm and can be considered slightly smaller than that by the DLS analysis because of ~1.5 nm thick Pt coating necessary for SEM imaging. Since the hydrophobic PS core of PDA-b-PS micelles cannot be swollen by water, the marginally larger diameter in the DLS result can be originated from the swollen corona of the PDA block in water, indicating that the part of PDA coronas is relatively thin in the spherical micelles. Thus, the PDA-b-PS micelle can be regarded as a PS particle covered by a thin PDA layer. The large difference in the block ratio of PDA to PS (1 to 14) also supports this description on the PDA-b-PS micelle as a PS particle with a thin PDA shell.

Since PDA-b-PS micelles consist of PS cores and PDA coronas, particles in Figure 3 should have dopamine functionality on their surface, indicating that we essentially produce dopamine-functionalized PS particles without additional modification of PS particles. To demonstrate utilization of the surface-functionalized PS particles, we first mixed these PS particles with an aqueous solution of $AgNO_3$ because dopamine can adsorb and reduce metal ions without a reducing agent [20]. As shown in Figure 4, the surface of PS particles is no longer smooth and has many small particles after the reaction with $AgNO_3$. In the enlarged image (the inset of Figure 3-4), each PS particle has 12~15 Ag nanoparticles with the diameter of ~10 nm, which is illustrated schematically in

Figure 3-4. The formation of Ag nanoparticles was supported by the observation of the absorption band at 450 nm in the UV-Vis spectrum due to the surface plasmon resonance of Ag nanoparticles (Figure 3-5(a)).

Since dopamine can strongly bind to the surface of metal oxides [21], we also effectively decorated PS particles, originated from PDA-b-PS micelles, with $TiO_2$ nanoparticles. In this case, we simply mixed dopamine-functionalized PS particles with $TiO_2$ nanoparticles in water. $TiO_2$ nanoparticles having the diameter of ~5 nm were used and are discernible on the surface of PS particles in both SEM and TEM images shown in Figure 3-6. A large number (~30) of $TiO_2$ nanoparticles were attached to each PS particle. These PS particles decorated with $TiO_2$ nanoparticles also exhibit the absorption maximum at 330 nm in the UV-Vis spectrum which is a characteristic of $TiO_2$ nanoparticles (Figure 3-5(b)). For a control experiment (not shown), PS particles produced from poly(acrylic acid)-b-polystyrene micelles, which have a similar diameter to that shown here but no dopamine functionality on the surface, were not decorated with $TiO_2$ nanoparticles, indicating that the dopamine functionality is crucial to bind oxide nanoparticles on PS particles.

## 3-4. Conclusion

Dopamine-functionalized PDA-b-PS was first derived from PPFPA-b-PS having activated esters which were synthesized by the RAFT polymerization. By inducing spherical micelles of amphiphilic PDA-b-PS in water, we obtained PS particles having dopamine functionality on their surface without additional surface modification. The block ratio of PS to PDA in the copolymer was large enough to induce spherical micelles of PS cores with short PDA coronas which are basically equivalent to PS particles with PDA surface. Thus, we were able to directly decorate these PS particles with Ag and $TiO_2$ nanoparticles due to the dopamine functionality on their surface.

## 3-5. References


[1] A. Roucoux, J. Schulz, H Patin, Chem. Rev. **2002**, 102, 3757.

[2] S.J. Oldenburg, R.D. Averitt, S.L. Westcott, N.J. Halas, Chem. Phys. Lett. **1998**, 288, 243

[3] L. Lu, I. Randjelovic, R. Capek, N. Gaponik, J. Yang, H. Zhang, A. Eychmuller, Chem. Mater. **2005**, 17, 5731.

[4] T. L. Kelly, M. O. Wolf, Chem. Soc. Rev. **2010**, 39, 1526.

[5] R. G. Chaudhuri, S. Paria, Chem. Rev. **2012**, 112, 2373.

[6] L. Lu, I. Randjelovic, R. Capek, N. Gaponik, J.H. Yang, H.J. Zhang, A. Eychmüller, Chem. Mater. **2005**, 17, 5731.

[7] B. Sadtler, A. Wei, Chem. Commun. **2002**, 15, 1604.

[8] Y. Liu, J. Goebla, Y. Yin, Chem. Soc. Rev. **2013**, 42, 2610.

[9] J. P. Raoa, K. E. Geckeler, Prog. Polym. Sci. **2011**, 36, 887.

[10] J.-H. Lee, D.-O. Kim, G.-S. Song, Y. Lee, S.-B. Jung, J.-D. Nam, Macromol. Rapid Commun. **2007**, 28, 634.

[11] F. Caruso, Adv. Mater. **2001**, 13, 11

[12] W.L. Shi, Y. Sahoo, M.T. Swihart, P.N. Prasad, Langmuir **2005**, 21, 1610.

[13] Z. Liang, A.S. Susha, F. Caruso, Adv. Mater. **2002**, 14, 1160.

[14] Y. Mai, A. Eisenberg, Chem. Soc. Rev. **2012**, 41, 5969

[15] K. Kataoka, A. Harada, Y. Nagasaki, Advanced Drug Delivery Reviews **2001**, 47, 113

[16] S. I. Yoo, S. H. Bae, K. S. Kim, B. H. Sohn, Soft Matter **2009**, 5, 2990

[17] J. Wang, W Li, J Zhu, Polymer **2014**, 55, 1079

[18] M. Eberhardt, R. Mruk, R. Zentel, P. Theato, Eur. Polym. J. **2005**, 41, 1569.

[19] Y. Liu, K. Ai, L. Lu, Chem. Rev. **2014**, 114, 5057.

[20] H. Lee, S. M. Dellatore, W. M. Miller, P. B. Messersmith, Science, **2007**, 318, 426.

[21] B. Oschmann, D. Bresser, M. N. Tahir, K. Fischer, W. Tremel, S. Passerini. R. Zentel, Macromol. Rapid Commun. **2013**, 34, 1693.

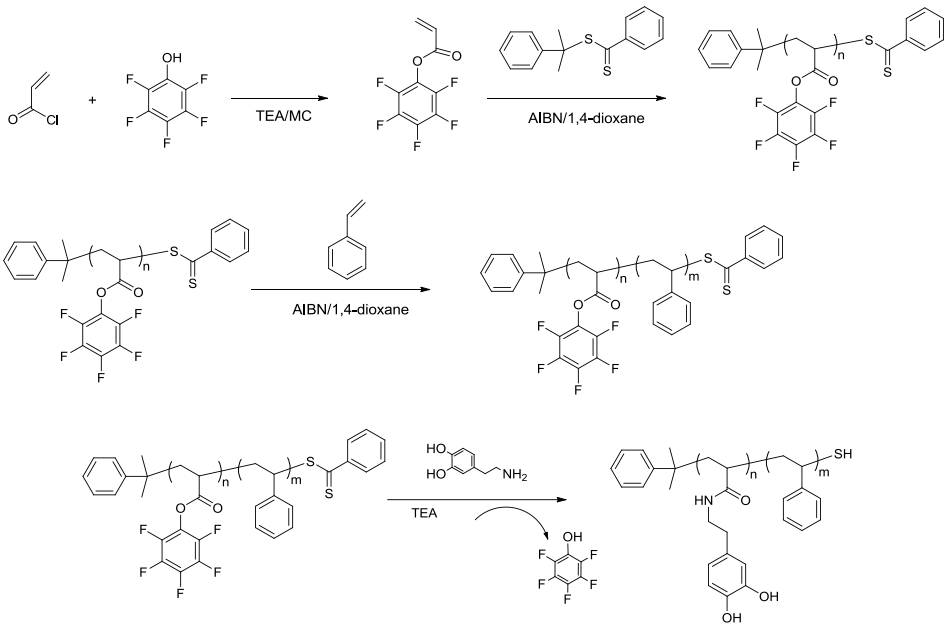


**Figure 3-1.** Synthesis of dopamine-functionalized PDA-b-PS from PPFPA-b-PS.

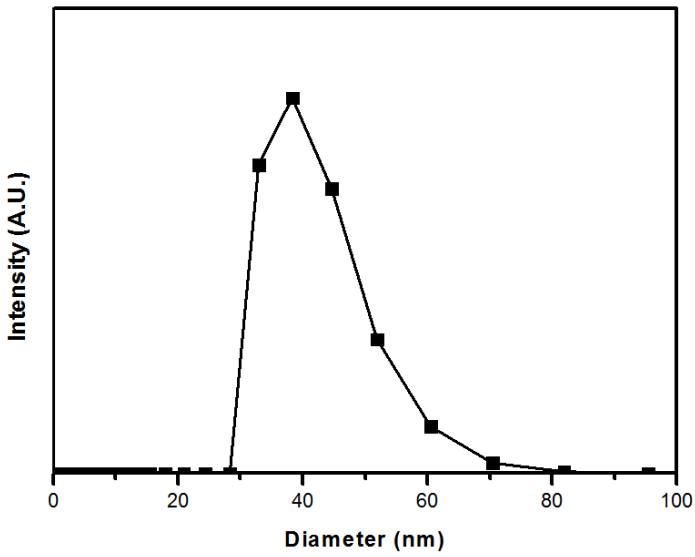


**Figure 3-2.** Size distribution of PDA-b-PS micelles by DLS measurements.

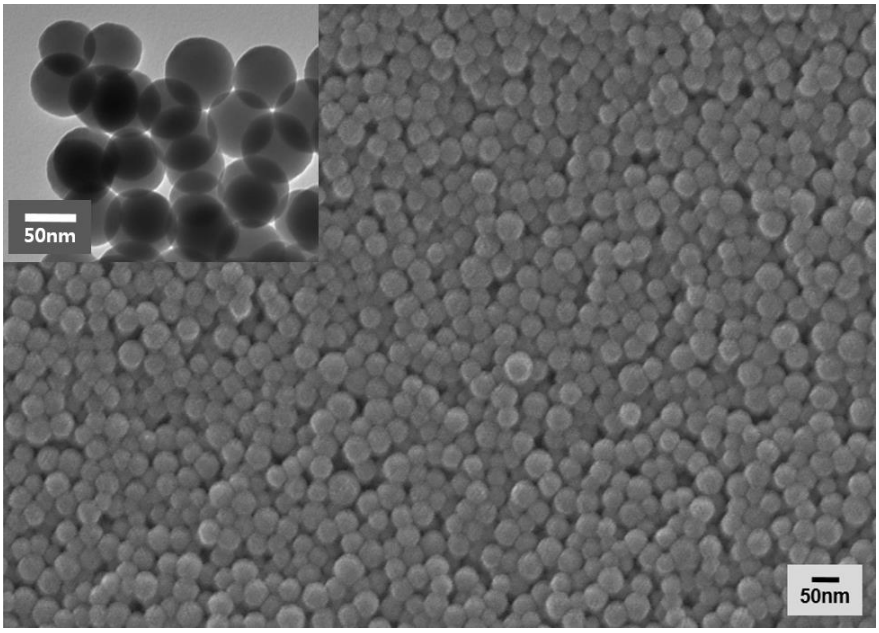


**Figure 3-3.** SEM and TEM (inset) images of PDA-b-PS micelles.

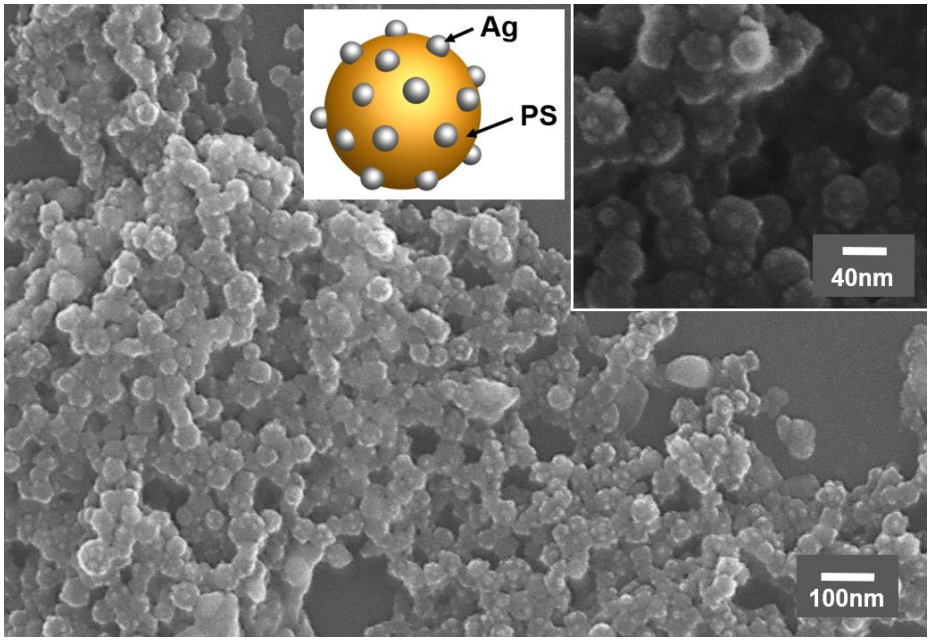


**Figure 3-4.** SEM image of PS particles decorated with Ag nanoparticles by utilizing PDA-b-PS micelles as dopamine-functionalized PS particles. The inset is an enlarged image.

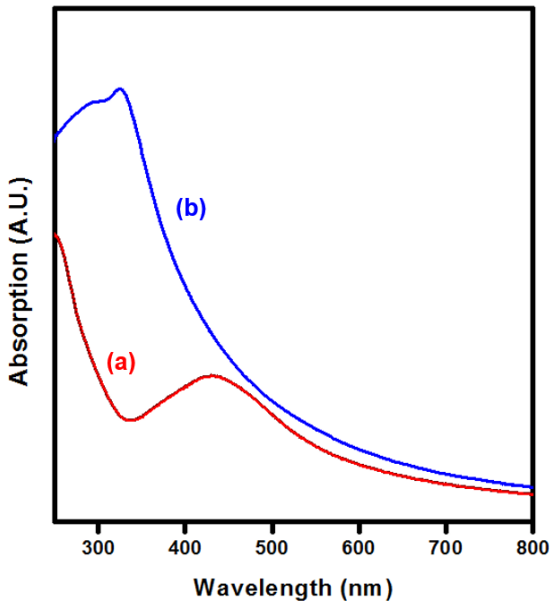


**Figure 3-5.** UV-Vis spectra of PS particles decorated with nanoparticles: (a) Ag; (b) $TiO_2$.

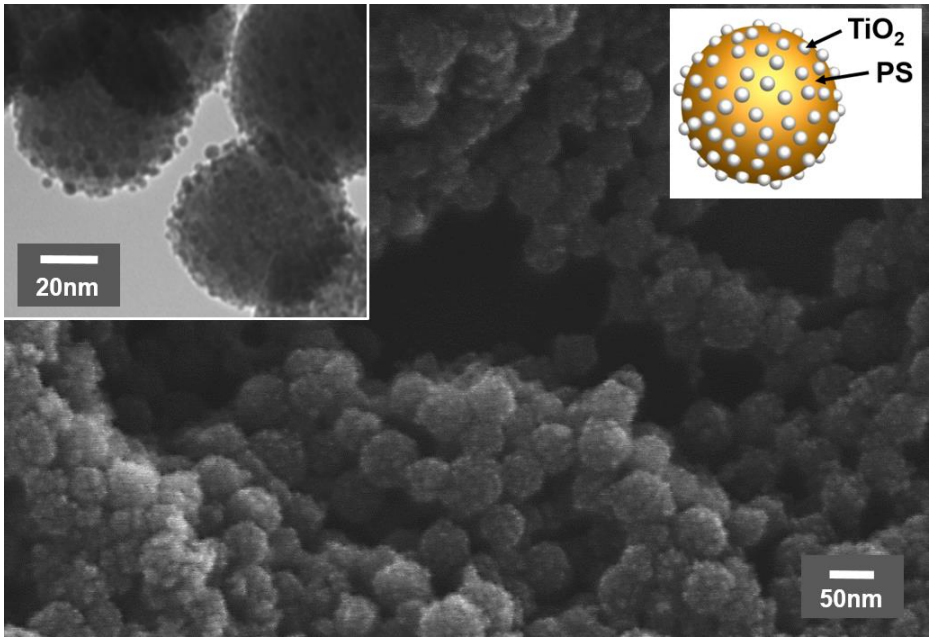


**Figure 3-6.** SEM image of PS particles with $TiO_2$ nanoparticles. The inset is a TEM image.

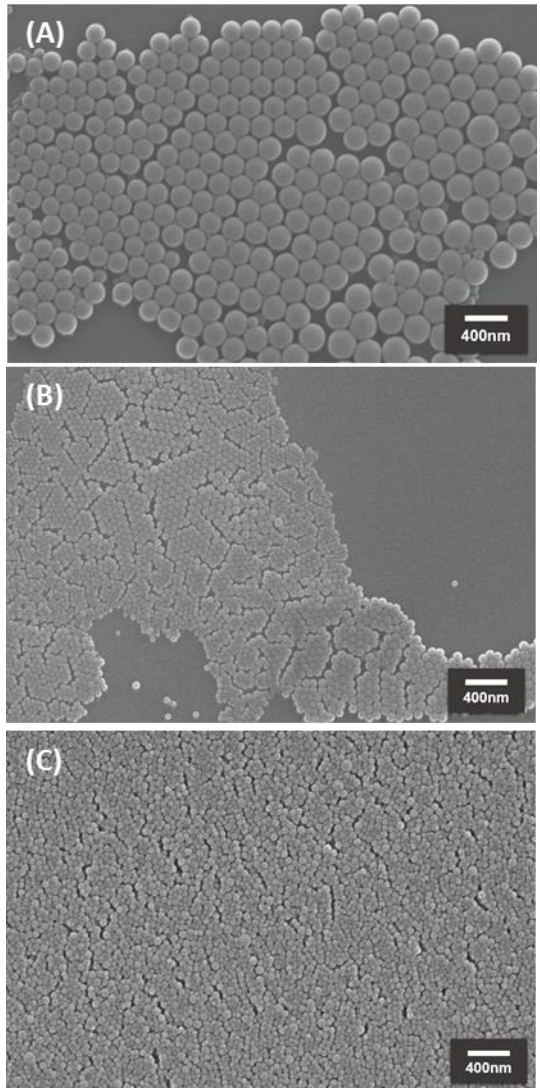


**Figure 3-7.** TEM images of PDA-b-PS micelles; (a) 4K-23K, (b) 9K-67K, (c) 4K-62K

# 국문요약

# 초구조콜로이드 사슬 및 표면이 기능화된 나노입자 제조를 위한 블록공중합체 마이셀의 합성

**이상화**

**화학부 고분자화학 전공**

**서울대학교 대학원**

나노사이즈의 빌딩블록의 조립을 통한 제어된 초분자구조는 나노사이즈 빌딩블록이 개별적으로 존재할 때와는 다르게 집합적인 전기적, 광자적, 자기적 특성을 나타내므로 기초과학에 매우 중요하다. 이와 같은 초분자구조는 균일한 금속, 반도체, 산화물, 고분자입자와 같이 다양한 물질을 통하여 입자간 제어된 인력을 통해 연구되어왔다.

잘 정의된 패치를 갖는 콜로이드 입자는 큰 범주에서 인위적인

원자구조의 원자가를 모사하는 일들로 발전되어 왔다. 그러나, 다중의 콜로이드 입자는 인위적으로 제어된 브랜치 및 가교구조로서는 아직까지 활용되지 않고 있다. 세 개의 블록으로 구성된 고분자 또는 두 개의 블록으로 구성된 고분자를 통하여 뚜렷한 패치 개수를 갖는 균일한 크기의 다중으로 구분되는 마이셀을 만들 수는 있으나, 이를 통한 제어된 브랜치 또한 가교된 초분자 중합은 아직 보고 되지 않았다.

본 논문에서는 우선 두 개의 블록으로 구성된 고분자를 통하여 세 개의 패치를 갖는 균일한 패치 마이셀을 만들었다. 그리고, 두 개의 기능성을 갖는 두 개의 패치를 갖는 마이셀과 함께 초분자 사슬을 만들었다. 세 개의 패치를 갖는 마이셀을 넣음으로써 초분자 사슬은 제어된 브랜치구조, 나아가서는 가교 및 네트워크 구조를 나타냈다. 대조적으로 두 개의 기능성을 갖는 경우에서는 긴 선형 초분자 사슬만이 만들어졌다. 패치 마이셀의 선형 사슬 및 네트워크 구조는 고전적인 고분자중합 및 젤화의 캐로더스 이론을 통하여 이해할 수 있다. 본 연구를 통하여 블록공중합체로부터 패치 마이셀의 합성을 근본적으로 이해하는 배

경을 제공하였고, 이를 토대로 가교된 고분자를 합성하는 것과 유사하게 나노크기의 패치 마이셀로부터도 가교된 초구조 사슬의 중합을 제어할 수 있음을 보여 초구조 합성의 범주를 확장하였다.

또한, 블록공중합체는 표면이 기능화된 입자로 활용될 수 있으며, 이와 같은 표면 기능화를 통하여 은, 이산화티탄 입자 등을 추가적인 표면처리 없이 도입할 수 있었다.

제 1장에서는 용액상에서 형성되는 블록공중합체 마이셀에 대해 개괄적으로 서술하였다. 기능성 블록공중합체를 위한 합성방법 및 후중합 반응에 관하여 간략히 소개하였다.

제 2장에서는 고분자를 통하여 세 개의 패치를 갖는 균일한 패치 마이셀을 제조하고 이를 통하여 제어된 브랜치구조, 나아가서는 가교 및 네트워크 구조를 형성할 수 있음을 확인하였고, 이는 고전적인 고분자중합 및 젤화의 캐로더스 이론을 통하여 이해할 수 있음을 확인하였다.

제 3장에서는 블록공중합체를 이용하여 표면이 기능화된 입자를 제조하여 그 표면의 기능기를 이용하여 은, 이산화티탄 입자

등의 금속입자 도입이 가능함을 확인하였다. 이를 통해 기존의 표면기능화 및 크기조절의 한계점을 극복할 수 있음을 확인하였다.

**핵심용어 : 이중블록공중합체, 자기조립, 초구조 고분자, 브랜치 구조, 네트워크 구조, 표면기능화, 나노입자, 도파민**

**학번 :** 2012-30878